Durham University

Durham E-Theses

Mathematical simulation of clay swelling due to water imbibition

WITHERS, CHARLOTTE

How to cite:

WITHERS, CHARLOTTE (2017) *Mathematical simulation of clay swelling due to water imbibition*, Durham theses, Durham University. Available at Durham E-Theses Online: http://etheses.dur.ac.uk/12128/

Use policy

The full-text may be used and/or reproduced, and given to third parties in any format or medium, without prior permission or charge, for personal research or study, educational, or not-for-profit purposes provided that:

- a full bibliographic reference is made to the original source
- a link is made to the metadata record in Durham E-Theses
- the full-text is not changed in any way

The full-text must not be sold in any format or medium without the formal permission of the copyright holders.

Please consult the full Durham E-Theses policy for further details.

Academic Support Office, The Palatine Centre, Durham University, Stockton Road, Durham, DH1 3LE
e-mail: e-theses.admin@durham.ac.uk Tel: +44 0191 334 6107
http://etheses.dur.ac.uk

Mathematical simulation of clay swelling due to water imbibition

Charlotte Withers

Thesis presented for the degree of

Master of Science by Research

Under the supervision of Dr. Simon Mathias

Department of Earth Sciences

Durham University

2017

Abstract

Clay minerals are commonly encountered in the drilling for oil and natural gas and have the potential to expand considerably when they come into contact with drilling fluids. Clay swelling is a significant issue in the drilling industry, leading to a number of borehole stability problems. This thesis develops a mathematical hydromechanical model to simulate the deformation due to swelling during capillary suction of water in unsaturated clays. The model builds on an existing modelling framework associated with coal shrinkage during coalbed methane extraction. Sorption of water in the model is represented by a Langmuir isotherm and a swelling strain term has been derived by adapting the theory of linear poroelasticity. The results show that for a clay plug with a low initial effective saturation ($S_{e0} = 0.001$) the amount of swelling correlates with clay content. These modelled results were compared with experimental swelling curves for two pure clay plugs and showed that, although the final swelling points converged, the swelling curves evolved at different rates. These findings indicate that further research is required before this model can be used to simulate clay swelling with a high degree of accuracy.

Contents

Abstract **i**

List of Figures **v**

List of Tables **vii**

Nomenclature **viii**

Key Equations **xii**

Acknowledgements **xv**

1 Introduction **1**

1.1 How clays swell 3

1.2 Simulation of clay swelling 6

1.2.1 Monte Carlo (MC) Simulations 7

1.2.2 Molecular Dynamics (MD) Simulations 8

1.2.3 Mixture Theory 9

1.2.4 Macroscopic swelling experiments 11

1.3 Coal Shrinkage 13

1.4 Thesis Aims 14

2 Methods & Data **15**

2.1 Conceptual Model 15

2.2 Mathematical Model 16

2.2.1 Recasting the equation in terms of the primary dependent variable 17

2.2.2 Hydraulic properties 18

2.2.3 The Langmuir adsorption isotherm 20

2.2.4 Parameterisation of the Langmuir isotherm for a clay swelling system . . . 22
2.2.5 Water density . . . 24
2.2.6 Bulk density . . . 24
2.2.7 Adaptation of the theory of linear poroelasticity . . . 28
2.2.8 Uniaxial strain assumption . . . 29
2.2.9 Saturated moisture content . . . 32
2.2.10 Maximum swelling strain . . . 36
2.2.11 Mapping elevation from a non-swelling domain to a swelling domain 37
2.3 Numerical Solution . . . 39
2.4 Data . . . 39

3 Results & Discussion 40
3.1 Capillary Suction Model . . . 40
3.2 Sorption Model . . . 44
3.2.1 Sensitivity Analysis . . . 46
3.3 Swelling Model . . . 47
3.3.1 Sensitivity Analysis . . . 50
3.3.2 Comparison with Experiments . . . 56

4 Future Research 60

5 Conclusions 62

6 Appendix A: Finite Difference Approximation 64

7 Appendix B: MATLAB Codes 66

8 Appendix C: ROSETTA Database 67

9 References **68**

List of Figures

2.1 Conceptual diagram of the clay plug. 16

2.2 Graph to show how S_{ef} has been determined. 23

3.1 Moisture content evolution with time for plugs containing (a) 5 % clay and (b) 30 % clay, with S_{e0} of 0.01. 41

3.2 Moisture content evolution with time for plugs containing (a) 5 % clay and (b) 30 % clay, with S_{e0} of 0.2. 42

3.3 Relationship between effective saturation and capillary pressure for a plug with a clay content of 5 % and a S_{e0} of 0.01. 43

3.4 Moisture content evolution with time for plugs containing (a) 5 % clay and (b) 30 % clay. 45

3.5 Variation of equilibrium time with s_F for four plugs with different clay contents. 46

3.6 Variation of equilibrium time with S_{ef} for four plugs with different clay contents. 47

3.7 Moisture content evolution and swelling curves for plugs containing 5 % clay and 15 % clay, with S_{e0} of 0.01. 49

3.8 Swelling curves for plugs containing (a) 5 % clay and (b) 15 % clay, with S_{e0} of 0.001. 50

3.9 Swelling curves for varying s_F for plugs containing (a) 5 % clay, (b) 10 % clay and (c) 15 % clay. 53

3.10 Swelling curves for varying S_{ef} for plugs containing (a) 5 % clay, (b) 10 % clay and (c) 15 % clay. 54

3.11 Swelling curves for varying ε_{sF} values for plugs containing (a) 5 % clay, (b) 10 % clay and (c) 15 % clay. 55

3.12 Comparison between model and experimental data for an illite plug. . . 56

3.13 Comparison between model and experimental data for a bentonite plug. 58

List of Tables

3.1 Capillary suction model parameters 40

3.2 Sorption model parameters 44

3.3 Swelling model parameters 48

3.4 Parameters used for comparison with illite swelling curve. 57

3.5 Parameters used for comparison with bentonite swelling curve. 59

Nomenclature

Greek Symbols

α	reciprocal of reference state pressure head [L^{-1}]
α_B	Biot coefficient [-]
β	Linear thermal expansion coefficient [K^{-1}]
β_m	Linear thermal expansion coefficient of clay matrix [K^{-1}]
$\boldsymbol{\varepsilon}$	Strain tensor
ε_b	Bulk strain [-]
ε_{b0}	Initial bulk strain [-]
$\varepsilon_{b,max}$	Maximum bulk strain [-]
ε_c	Strain of clay matrix [-]
ε_s	Swelling strain [-]
ε_{s0}	Initial swelling strain [-]
$\varepsilon_{s,max}$	Maximum swelling strain [-]
ε_{sF}	Factor by which $\varepsilon_{b,max}$ is greater than the observed maximum negative vertical strain [-]
η	Empirical exponent [-]
θ	Moisture content [-]
θ_I	Initial moisture content [-]
θ_r	Residual moisture content [-]
θ_s	Saturated moisture content [-]
λ	Lamé coefficient [$ML^{-1}T^{-2}$]
ν	Poisson's ratio [-]
ρ_a	Density of air [ML^{-3}]
ρ_b	Bulk density [ML^{-3}]
ρ_{dc}	Density of dry clay matrix [ML^{-3}]

ρ_w	Density of water [ML^{-3}]
ρ_{w0}	Initial density of water [ML^{-3}]
$\boldsymbol{\tau}$	Stress tensor
$\boldsymbol{\tau'}$	Effective stress tensor
τ'	Effective stress [$ML^{-1}T^{-2}$]
τ_m	Trace of stress tensor [$ML^{-1}T^{-2}$]
ϕ	Porosity [-]
ϕ_0	Initial porosity [-]
ψ	Pressure head [L]

Latin Symbols

c	mass of pore-water per unit volume of pore-space [ML^{-3}]
C_{bp}	Bulk pore compressibility [$M^{-1}LT^2$]
C_F	Fluid compressibility [$M^{-1}LT^2$]
C_R	Rock compressibility [$M^{-1}LT^2$]
E	Young's modulus [$ML^{-1}T^{-2}$]
g	Acceleration due to gravity [LT^{-2}]
G	Shear modulus [$ML^{-1}T^{-2}$]
h	Hydraulic head [L]
H	Height of clay plug [L]
H_I	Initial height of clay plug [L]
H_{max}	Maximum height achieved by clay plug [L]
K	Bulk modulus [$ML^{-1}T^{-2}$]
K_m	Bulk modulus of clay matrix [$ML^{-1}T^{-2}$]
K_d	Linear isotherm partition coefficient [$M^{-2}L^3$]
K_s	Saturated hydraulic conductivity [LT^{-1}]

K_z	Hydraulic conductivity in z-direction [LT^{-1}]
M	Constrained axial modulus [$ML^{-1}T^{-2}$]
M_a	Mass of air [M]
M_b	Bulk mass [M]
M_{dc}	Mass of dry clay matrix [M]
M_w	Mass of water [M]
M_{wp}	Mass of water stored in the pore-space [M]
M_{ws}	Mass of water sorbed by the clay [M]
n	Empirical exponent [-]
P	Confining pressure [$ML^{-1}T^{-2}$]
P_a	Air pressure [$ML^{-1}T^{-2}$]
P_c	Capillary pressure [$ML^{-1}T^{-2}$]
P_p	Pore pressure [$ML^{-1}T^{-2}$]
P_{p0}	Initial pore pressure [$ML^{-1}T^{-2}$]
P_w	Water pressure [$ML^{-1}T^{-2}$]
P_{w0}	Initial water pressure [$ML^{-1}T^{-2}$]
q	Rate of flow of water into clay plug per unit area [LT^{-1}]
s	Mass of water sorbed per unit mass of clay [-]
s_I	Initial mass of water sorbed per unit mass of clay [-]
s_{max}	Maximum sorption capacity [-]
s_F	Describes how much water is adsorbed as a multiple of the maximum mass of water that can be stored in the pore-space [-]
S_e	Effective saturation [-]
S_{e0}	Initial effective saturation [-]
S_{ef}	Fraction of S_e where maximum adsorption has almost occurred [-]
S_w	Water saturation [-]

S_{w0}	Initial water saturation [-]
t	Time [T]
V_b	Bulk volume [L^3]
V_c	Volume of wet clay matrix [L^3]
V_{dc}	Volume of dry clay matrix [L^3]
V_p	Volume of pore-space [L^3]
V_{wp}	Volume of water stored in the pore-space [L^3]
V_{ws}	Volume of water sorbed by the clay [L^3]
z	Elevation [L]

Key Equations

Listed below are the key equations used in this thesis. Most of the later equations in this thesis have been derived from these key equations.

Mass conservation statement (p.16)

$$\frac{\partial m_w}{\partial t} = \frac{\partial}{\partial t}(\rho_w \theta + \rho_b s) = -\frac{\partial}{\partial z}(\rho_w q)$$

Mass conservation statement in terms of the primary dependent variable, P_w (p.17)

$$\frac{\partial P_w}{\partial t} = -\frac{\partial}{\partial z}(\rho_w q)\left[\rho_w \frac{\partial \theta}{\partial P_w} + \theta \frac{\partial \rho_w}{\partial P_w} + s\frac{\partial \rho_b}{\partial P_w} + \rho_b \frac{\partial s}{\partial P_w}\right]^{-1}$$

Hydraulic properties (p.18-20)

$$S_e = (1 + |\alpha\psi|^n)^{-m}$$

$$K_z = K_s {S_e}^{\eta}[1 - (1 - {S_e}^{1/m})^m]^2$$

$$\theta = (\theta_s - \theta_r)S_e + \theta_r$$

$$h = \psi + z$$

$$\psi = \frac{P_w}{\rho_w g}$$

Flow rate per unit area (p.18)

$$q = -K_z \frac{\partial h}{\partial z}$$

Langmuir isotherm for clay swelling system (p.22)

$$\frac{s}{s_{max}} = \frac{K_d c}{s_{max} + K_d c}$$

Stress-strain relationship for poroelastic and thermoelastic medium (p.28)

$$\boldsymbol{\varepsilon} = \frac{1}{2G}\boldsymbol{\tau} - \frac{\nu}{2G(1+\nu)}\mathrm{trace}(\boldsymbol{\tau})\boldsymbol{I} - \left(\frac{C_{bp}}{3}P_p + \beta\vartheta\right)\boldsymbol{I}$$

"The copyright of this thesis rests with the author. No quotation from it should be published without the author's prior written consent and information derived from it should be acknowledged."

Acknowledgements

I would like to thank my supervisor Dr. Simon Mathias for giving me this opportunity and for all of his guidance and support this year. He has helped to make the transition from undergraduate to postgraduate study as smooth as possible, for which I am incredibly grateful. I look forward to working with him in the future.

My thanks also go to Helena, Jack, Ayo, Salim and Cath for their help and patience with introducing me to MATLAB, and for the intellectual (and sometimes not so intellectual) discussions.

I would not be where I am today without the support from my family. They have always encouraged me to follow my ambitions and are there for me when I need them.

To Laura, Milly, Rose, Bob, Ellie, Sarah and Rosie, thank you for putting up with me and always making me laugh. You're the best friends anyone could ask for. None of this could have been possible without your support and friendship.

Finally, I would like to thank the staff and students in the Earth Sciences department at Durham University for providing me with a friendly and (at times very entertaining) working environment. There's no place I'd rather be.

1 Introduction

Mudrocks comprise up to 55 % of sedimentary rock successions and are deposited in a range of environments, thus making them the most abundant lithology globally (Tucker, 2001). They can act as either source rocks or impermeable cap rocks to reservoir formations and are therefore commonly encountered in the drilling for oil and natural gas (Anderson et al., 2010). One of the main constituents of mudrocks is clay (Tucker, 2001). Clays are layered minerals which have the potential to expand considerably when hydrated (Anderson et al., 2010). This process, known as clay swelling, occurs when drilling fluids interact with clay-bearing mudrocks and is estimated to cost the drilling industry up to $1 billion annually (Wilson & Wilson, 2014). Drilling fluids are a vital component in the drilling of a borehole, performing tasks such as lubricating the drill bit and maintaining pressure down the borehole (Anderson et al., 2010). The majority of fluids currently in use are water-based in composition (Anderson et al., 2010). Although safer for the environment than previously used oil-based fluids, the interaction between water-based drilling fluids and surrounding mudrock can lead to significant clay swelling (Anderson et al., 2010). More than 70 % of borehole stability problems are thought to be associated with clay swelling (Lal, 1999), including bit-balling, where pieces of mudrock become stuck to the drill bit, and clogging of flow lines due to the inclusion of mud cuttings (Wilson & Wilson, 2014). In exceptional cases swelling can cause the walls of the borehole to cave in, leading to abandonment of the borehole entirely (Wilson & Wilson, 2014; Anderson et al., 2010).

In 2014 oil and natural gas comprised two of the largest energy supplies globally (IEA, 2016). Global energy consumption is predicted to increase by up to 32.5 % by 2040 (based on 2014 levels), with oil and gas remaining as significant sources of energy (IEA, 2015). As a result, there will be continued demand for the exploration

and drilling of new reserves. In order to minimise the effect of clay swelling on drilling operations, a lot of research is focussed on understanding the mechanisms of swelling and developing effective inhibitors. Of particular interest is the work currently being undertaken by the Layered Mineral Geochemistry Group at Durham University. They are investigating how the chemical properties of different solutions affect the degree of swelling undergone by different types of clay (e.g. Erdogan, 2016). This work is vital towards the development of effective swelling inhibitors and thereby cutting the costs incurred by the drilling industry as a result of borehole instability. The aim of this thesis is to develop a numerical model to accompany the macroscopic swelling experiments performed by the Layered Mineral Geochemistry Group at Durham University.

1.1 How clays swell

Clays belong to the phyllosilicate group and are primarily formed through weathering and soil formation (Chamley, 1989, p.3). Clay minerals are layered structures, containing cations which undergo isomorphic substitutions, resulting in each layer to become negatively charged (Anderson et al., 2010). These layers are then stacked in either an alternating tetrahedral-octahedral arrangement (1:1 clays), or with an octahedral sheet sandwiched between two tetrahedral sheets (2:1 clays) (Skipper et al., 2006; Anderson et al., 2010). Exchangeable cations reside in the region between sheets, known as the interlayer region, thereby balancing the negative charge of the layers (Smith et al., 2006). The exchangeable nature of these cations allows for the introduction of water which can lead to significant swelling of the clay mineral (Karaborni et al., 1996).

Clay swelling occurs via two mechanisms. The first is known as crystalline swelling and takes place in all types of clay (Anderson et al., 2010). Water is adsorbed by the interlayer region, resulting in the hydration of interlayer cations and subsequent formation of hydrate layers (Boek et al., 1995; Anderson et al., 2010). These hydrate layers force the mineral layers apart, thus leading to expansion of the clay mineral (Boek et al., 1995). There is a limit to the number of hydrate layers which form within the interlayer region (Boek et al., 1995) and therefore crystalline swelling tends to result in microscopic expansion of clay. The second mechanism of swelling is known as osmotic swelling and only occurs in clay minerals where there is a difference in ionic concentration between the interlayer region and surrounding pore-water (Boek et al., 1995; Anderson et al., 2010). Water is consequently taken in by the interlayer region to re-establish equilibrium (Boek et al., 1995). The amount of water adsorbed in this case is considerably higher and can therefore lead to greater expansion than crystalline swelling (Anderson et al., 2010). For example, osmotic swelling in Na^+-saturated smectites is so significant that it can cause borehole instability (Anderson et

al., 2010).

A number of factors dictate the swelling capacity of a clay mineral. One such factor is the mineral layer substitution type. Hensen & Smit (2002) ran Monte Carlo simulations (see Section 1.2.1) on Na-montmorillonite which undergoes octahedral substitutions and Na-beidellite which undergoes tetrahedral substitutions. They showed that the montmorillonite forms three hydrate layers, whereas the beidellite is limited to a single hydrate layer (Hensen & Smit, 2002; Anderson et al., 2010). This is because the cations in the beidellite are bonded to the clay surface so strongly that it is not possible to fully hydrate them, and therefore, no matter how much water vapour pressure is applied, the mineral will not expand any further than the first hydrate layer (Hensen & Smit, 2002).

Another factor which affects degree of swelling is the hydration energy of interlayer cations. It has been shown through x-ray diffraction (XRD) experiments that for a group of clay minerals with monovalent interlayer cations, those with higher hydration energies result in more swelling than those with lower energies (Norrish, 1954; Anderson et al., 2010). This is believed to be because a high hydration energy allows for migration of the cations towards the mid-region of the interlayer, thus increasing interlayer spacing (Hensen & Smit, 2002). Although polyvalent cations generally have higher hydration energies, the relationship with swelling is not as clear (Norrish, 1954; Anderson et al., 2010).

Cation charge also impacts swelling capacity. In general, clays which contain divalent cations in their interlayer regions exhibit less swelling than those containing monovalent cations (Anderson et al., 2010). This is because the increased charge means that the clay mineral as a whole is more stable and is therefore less likely to swell (Anderson et al., 2010). There are some exceptions, however. For example, Ca-bearing clays experience greater swelling than those containing K^+ ions because the majority of Ca^{2+}

ions will fully hydrate and migrate into the centre of the interlayer region, leading to an increase in interlayer spacing (Anderson et al., 2010). In contrast, K^+ ions do not fully hydrate and migrate towards the clay surface instead (Boek et al., 1995; Anderson et al., 2010), thus resulting in less swelling.

The permeability of the clay-bearing mudrock is also a significant factor in the study of clay swelling. Swelling is often greater in rocks containing cracks or fissures which allow water to flow through easily and therefore lead to more adsorption (Franklin & Dusseault, 1989, p.332). Less swelling is likely to occur in mudrocks which have a low permeability, such as those which are well cemented, for example with organic matter or calcite (Franklin & Dusseault, 1989, p.332).

1.2 Simulation of clay swelling

The first clay swelling experiments were undertaken in 1933 (Karaborni et al., 1996), and since then a variety of techniques have been developed, depending on the focus of the research. For example, x-ray diffraction is used to measure the change in inter-layer spacing due to water adsorption, and therefore determine whether crystalline or osmotic swelling has taken place (Amorim et al., 2007; Anderson et al., 2010). Neutron scattering is used to determine the structural and compositional properties of a swelling complex (Skipper et al., 2006). The macroscopic swelling capacity of a clay mineral can be investigated by introducing an aqueous solution to a clay specimen and measuring the height or volume increase with time (Anderson et al., 2010; Erdogan, 2016).

Although experimental techniques are useful for investigating a number of swelling properties and processes, it can be difficult to make accurate interpretations due to the challenge of reproducing borehole conditions and the fact that clay minerals range widely in composition (Anderson et al., 2010). As such, laboratory experiments are often coupled with modelling techniques. Modelling techniques are useful for studying the processes involved in clay swelling at the microscopic level, something that is not always possible using experimental methods (Boek et al., 1995). For example, smectites are comprised of small platelets and therefore cannot be investigated using x-ray or neutron diffraction experiments alone (Boek et al., 1995). Modelling techniques are also useful for simulating extreme pressure and temperature conditions that would be impractical to achieve in a laboratory environment (Allen & Tildesley, 1987, p.5).

Three techniques employed in the modelling of clay swelling are the Monte Carlo (MC) method, the Molecular Dynamics (MD) method and Mixture Theory, and are discussed in greater detail below.

1.2.1 Monte Carlo (MC) Simulations

The principle underlying MC simulations is statistical mechanics (Anderson et al., 2010; Boek et al., 1995). A mathematical model is built using potential functions to represent molecular interactions (Boek et al., 1995; Skipper et al., 1995) and simulations are performed across a range of parameter inputs in order to define the system's equilibrium properties (Boek et al., 1995). Results are then calibrated with experimental data (Skipper et al., 1995).

MC simulations are particularly useful for the modelling of interlayer spacing changes with increasing water content. For example, Boek et al. (1995) ran simulations in the isothermal-isobaric ensemble (pressure, temperature and number of particles held constant) in order to examine the swelling mechanisms of Na-, Li- and K-montmorillonites. Water content was increased in small increments to assess the impact on interlayer spacing in greater detail (Boek et al., 1995). They observed that, with increasing water content, the Na^+ and Li^+ ions are fully hydrated, become detached from the clay surface and migrate to the centre of the interlayer region, forming a diffuse ion swarm and increasing the interlayer spacing in a stepwise manner. The K^+ ions, by comparison, only partially hydrate and instead migrate towards the clay surface (Boek et al., 1995). Their simulations showed good agreement with experimental swelling curves and the work on K^+ ions in particular has been vital in aiding the development of swelling inhibitors.

Chávez-Páez et al. (2001) investigated the effects of constant normal stress and constant chemical potential on the swelling mechanisms of a Wyoming Na-montmorillonite. They found that under constant normal stress conditions up to five hydrate layers form in the interlayer region, depending on the water content. They also found that when chemical potential is held constant swelling is nonuniform; variations in the basal spac-

ing result in variations in the amount of water adsorbed, and therefore the amount of swelling undergone.

The ability to perform MC simulations under a variety of ensembles, and therefore assess the impact of different parameters, highlights an advantage of using this method to investigate clay swelling. A drawback of traditional MC methods, however, is that they do not consider Newton's equations of motion which makes it difficult to gain any dynamical information (Kukol, 2008, p.26). As such, MC simulations are often accompanied by MD techniques to obtain a more complete overview of swelling.

1.2.2 Molecular Dynamics (MD) Simulations

MD simulations are performed in order to determine the dynamic properties of a clay swelling system (Allen & Tildesley, 1987, p.71). This is done by assigning each particle in the system with an initial position and velocity, and then solving Newton's equations of motion in order to model how the system progresses with time (Bleam, 1993; Anderson et al., 2010). A major advantage of running MD simulations is that this temporal evolution allows for comprehensive comparisons to be made with experimental methods, such as Fourier transform infrared spectroscopy and nuclear magnetic resonance (Anderson et al., 2010; Suter et al., 2009). However, systems in MD simulations are often restricted to certain ensembles, therefore limiting the number of potential parameters which can be tested (Anderson et al., 2010). As such, MD simulations are commonly run in conjunction with MC methods (Anderson et al., 2010). It is common to find that the initial states used in MD simulations are actually the equilibrium properties determined by MC techniques (Chang et al., 1998). This was the approach taken by Chang et al. (1997) who ran MC simulations to determine the equilibrium conditions which they then used in MD simulations to investigate the interlayer molecular structure of Wyoming Li-montmorillonite with varying hydrate layers. They found that

for the one and two hydrate layer systems, where the interlayer species are immobile, the MC simulations were appropriate for defining initial conditions. By comparison, the MC simulations were not appropriate for the three hydrate layer system, and instead MD methods were employed (Chang et al., 1997).

Tambach et al. (2004) combined MC and MD simulations in the grand canonical ensemble (volume, temperature and chemical potential held constant) to examine how relative humidity affects the swelling behaviour of Wyoming and Arizona montmorillonite minerals. MD simulations were run to displace interlayer cations and any water molecules already present in the interlayer region, followed by MC simulations to inject additional water molecules (Tambach et al., 2004). Their results highlighted the dependence of the amount of water in the interlayer region on the clay species, type of exchangeable cation present and relative humidity.

Karaborni et al. (1996) examined the swelling capacity of Na-montmorillonite. Performing a combination of MC and MD simulations they increased the interlayer spacing discretely, holding it constant following each increase to allow for water molecules to enter or leave the interlayer region until equilibrium conditions were achieved. Their findings indicate that following the introduction of water into the interlayer region one, three and five hydrate layers formed, in contrast with the expected formation of one, two, three then four layers. Rather than forming sequentially, they found that the second and third hydrate layers formed simultaneously, as did the fourth and fifth layers.

1.2.3 Mixture Theory

Mixture theory, sometimes known as continuum theory, is used to study multi-phase fluid flow in porous media and can be applied to the study of clay swelling systems (Bennethum et al., 1997; Hassanizadeh & Gray, 1990; Bennethum, 2007). Unlike MD and MC methods which focus on clay swelling on the microscopic scale, mixture theory

operates on the macroscopic scale (Hassanizadeh & Gray, 1990). The principle behind this method is that the system under investigation is treated as a mixture and each component of the system as a continuum which exists everywhere in the domain being studied (Hassanizadeh & Gray, 1979; Bennethum & Cushman, 1996; Lemon et al., 2006). Together these components are treated as overlaying continua (Bennethum et al., 1997; Hassanizadeh & Gray, 1979). Macroscale conservation statements are developed to include terms that take into account the interactions between continua (Murad et al., 1995; Bennethum et al., 1997; Weinstein et al., 2008). Relevant constitutive equations can then be incorporated and together the set of equations is solved to simulate the process under investigation (Hassanizadeh & Gray, 1990). The advantage of working on the macroscale is that any assumptions that are required can be introduced at this level and the model becomes more applicable to real life situations (Hassanizadeh & Gray, 1990). On the other hand, because this approach considers only the macroscale, some microscale properties of the system are not taken into account, thus resulting in the possibility of unnecessary assumptions being made (Hassanizadeh & Gray, 1990). In order to tackle this disadvantage, the hybrid mixture theory has been developed, e.g. Hassanizadeh & Gray (1979), Bennethum & Cushman (1996). In this case microscale conservation equations are introduced first, then averaged spatially and upscaled to produce macroscale conservation equations (Bennethum et al., 1997).

The hybrid mixture theory has been adopted by Bennethum et al. (1997), who adapt Darcy's Law, Terzaghi's Effective Stress Principle and Fick's First Law to develop a generalised set of governing equations to simulate clay swelling. They adopt a two-scale, two-phase system: the microscale represents the clay platelets and vicinal water, and the macroscale represents individual clay particles (made up of the platelets and water). The solid clay platelets and the liquid vicinal water are treated as overlaying continua (Bennethum et al., 1997). Conservation statements are developed at the microscale and

are averaged to produce macroscale equations, meaning that the microscale properties are not lost or ignored (Bennethum et al., 1997).

Mixture theory techniques have also been applied to simulate other swelling media. For example, Lemon et al. (2006) applied a mixture theory to model in-vitro tissue growth, an important process in therapeutic tissue engineering. In their model all tissue components are considered as continua, all simultaneously existing in the same space (Lemon et al., 2006). Mass and force conservation equations are defined on the macroscopic scale for each component and constitutive equations are developed to define how stress affects material deformation (Lemon et al., 2006). Their results show good agreement with experimental studies and highlight areas where further research in the field is required.

Weinstein et al. (2008) developed a hybrid mixture theory to simulate swelling drug delivery systems. The drug is carried inside a polymer through the body and as bodily fluids interact with the polymer it swells and the drug can be extracted (Weinstein et al., 2008). Their system is comprised of three phases on the microscale: a polymer phase, a drug phase and a liquid phase, which are treated as a homogeneous mixture on the macroscale (Weinstein et al., 2008). Conservation statements are developed for each phase and upscaled to produce macroscale equations and the Coleman-Noll method is used to derive relevant constitutive relations (Weinstein et al., 2008; Bennethum et al., 1996). The advantage of this model is that it has been kept non-specific to allow for its application to other swelling media (Weinstein et al., 2008).

1.2.4 Macroscopic swelling experiments

A number of experimental techniques have also been developed to investigate the macroscopic swelling behaviour of clay minerals. Erdogan (2016) examined the impact of different salt solutions and organic solvents on the swelling behaviour of illite and

bentonite samples. Linear expansion was monitored using a non-contact linear displacement meter (Erdogan, 2016). Following a similar method, Zhang & Sun (1999) ran swelling tests on a clay containing 96 % wt Ca-montmorillonite to determine how hydroxyethylcellulose, a drilling additive, can be improved as a clay swelling inhibitor. In both studies the samples were first compressed to form plugs, which were then placed into chambers and the test solutions introduced.

Taking a slightly different approach, Besq et al. (2003) investigated the swelling capacity of bentonite by adding the powdered sample directly to a cylinder containing the test solution over the course of 4 hours. The volume of swollen bentonite was then measured after 24 hours (Besq et al., 2003).

The aim of the model in this thesis is to focus on macroscopic swelling directly, thereby eradicating any uncertainty associated with upscaling results. The model builds on coal matrix shrinkage models which are able to simulate coal shrinkage due to methane desorption on a regional scale (e.g. Shi & Durucan, 2004), as will be discussed in Section 1.3.

1.3 Coal Shrinkage

The principle underlying the clay swelling model developed in this thesis is based on the mechanism of coal shrinkage due to methane desorption.

Coal seams are comprised of a dual porosity system: (1) a well-defined, naturally occurring fracture system, known as a cleat network, and (2) a highly heterogeneous microporous coal matrix (Shi & Durucan, 2004; Pillalamarry et al., 2011). Coal seams contain a large, potentially recoverable amount of methane, and up to 95 % of this gas is found adsorbed to the internal surfaces of the microporous matrix (Levine, 1996; Pillalamarry et al., 2011). The cleat system is often saturated with water, which prevents the methane from desorbing (Pillalamarry et al., 2011). During the extraction of methane, water is pumped from the coalbed, leading to a decrease in pressure and consequently desorption from the internal coal surfaces (Cui & Bustin, 2005; Pillalamarry et al., 2011). The methane diffuses from the micropores to the cleat network and flows to the production well (Cui & Bustin, 2005). The process of methane desorption results in shrinkage of the coal matrix (Palmer & Mansoori, 1998).

Various models have been developed to investigate the mechanisms of gas desorption and how permeability, in particular, is affected by coal shrinkage. Shi & Durucan (2004) have adapted the theory of linear poroelasticity to develop a model investigating how cleat permeability varies with pore-pressure during gas desorption. They derived stress-strain relationships to represent a linear elastic gas-desorbing porous medium and replaced a thermal expansion term with a matrix shrinkage term (Shi & Durucan, 2004). The clay swelling model in this thesis follows a similar approach, by deriving stress-strain relationships and incorporating a swelling term to simulate the expansion of clay due to water imbibition.

1.4 Thesis Aims

The aim of this project is to develop a mathematical hydromechanical model to simulate the deformation due to swelling during water imbibition in unsaturated clays. The model builds on an existing modelling framework associated with coal matrix shrinkage due to coalbed methane extraction. In contrast to the models discussed previously which tend to focus on the microscopic level of clay swelling, this model investigates macroscopic expansion of clay, and will accompany macroscopic swelling experiments performed by the Layered Mineral Geochemistry Group at Durham University.

This model considers both the migration of bulk pore-water through the plug and the adsorption of water between the clay mineral layers. Sorption is represented by a Langmuir isotherm. In order to incorporate expansion of the plug due to sorption, a swelling strain term is derived by adapting the theory of linear poroelasticity under uniaxial strain conditions.

Once developed, the model is compared with experimental results previously obtained by Erdogan (2016). Finally, recommendations are made for future research.

2 Methods & Data

2.1 Conceptual Model

A mathematical model is developed to simulate the deformation that occurs when water enters and migrates through a one-dimensional unsaturated clay plug, as described in Figure 2.1. The plug is assumed to be homogeneous and does not contain any cracks or fissures. The pore-space of the plug is a multi-phase system containing water and air (Schwartz & Zhang, 2003, p.130; Bear & Cheng, 2010). An unsaturated setting is assumed, which means a negative pressure head occurs. This is because water is held in the pore-space under surface tension forces which occur at the interface between water and air (Allan Freeze & Cherry, 1979). A fixed water table condition is applied at the base of the plug, by imposing a 0 cm pressure head. Water is sucked vertically up the plug by the action of capillary rise and is split up into two components: (1) bulk pore-water which migrates through the pore-space via capillary rise, and (2) water which is adsorbed between the clay mineral layers. This adsorption forces the clay layers apart and leads to macroscopic expansion of the plug. Deformation is assumed to be elastic and occurs under uniaxial strain conditions.

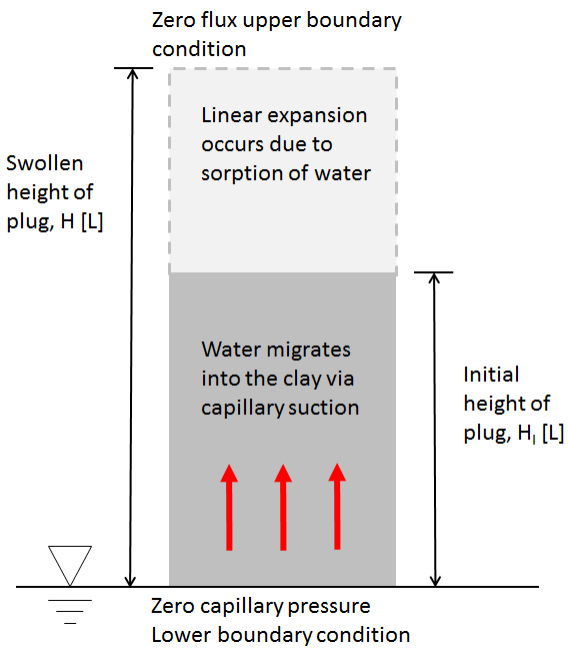

Figure 2.1: Conceptual diagram of the clay plug.

2.2 Mathematical Model

Mass conservation states that the flow of water into the clay plug is equal to the change in storage of water within the plug.

A mass conservation statement for the clay swelling system can be written as follows

$$\frac{\partial m_w}{\partial t} = \frac{\partial}{\partial t}(\rho_w \theta + \rho_b s) = -\frac{\partial}{\partial z}(\rho_w q) \tag{1}$$

subject to the following initial and boundary conditions

$$\theta = \theta_I, \quad 0 \leq z \leq H(t), \quad t = 0 \tag{2}$$

$$\theta = \theta_s, \quad z = 0, \quad t > 0 \tag{3}$$

$$s = s_I, \quad 0 \leq z \leq H(t), \quad t = 0 \tag{4}$$

$$s = s_{max}, \quad z = 0, \quad t > 0 \tag{5}$$

$$q = 0, \quad z = H(t), \quad t > 0 \tag{6}$$

where θ [-] represents the moisture content, θ_I [-] and θ_s [-] represent the initial and saturated moisture content respectively, s [-] represents the mass of water sorbed per unit mass of clay (comprising the clay matrix, water and air), s_I [-] and s_{max} [-] represent the initial mass of water sorbed and the maximum adsorption capacity respectively, ρ_w [$\mathrm{ML^{-3}}$] and ρ_b [$\mathrm{ML^{-3}}$] represent the water and bulk density respectively, q [$\mathrm{LT^{-1}}$] represents the flow rate of water into the clay plug, z [L] represents the elevation of the plug, H [L] represents the height of the plug and t [T] represents time.

2.2.1 Recasting the equation in terms of the primary dependent variable

When solving partial different equations, such as Eq.(1), it is necessary to define a primary dependent variable (PDV) to solve for. In this model water pressure, P_w [$\mathrm{ML^{-1}T^{-2}}$], has been chosen as the PDV.

Applying the product rule to the mass conservation equation, Eq.(1), and recasting in terms of P_w leads to

$$\rho_w \frac{\partial \theta}{\partial P_w}\frac{\partial P_w}{\partial t} + \theta \frac{\partial \rho_w}{\partial P_w}\frac{\partial P_w}{\partial t} + s\frac{\partial \rho_b}{\partial P_w}\frac{\partial P_w}{\partial t} + \rho_b \frac{\partial s}{\partial P_w}\frac{\partial P_w}{\partial t} = -\frac{\partial}{\partial z}(\rho_w q) \tag{7}$$

Rearranging for $\partial P_w/\partial t$ gives

$$\frac{\partial P_w}{\partial t} = -\frac{\partial}{\partial z}(\rho_w q)\left[\rho_w \frac{\partial \theta}{\partial P_w} + \theta \frac{\partial \rho_w}{\partial P_w} + s\frac{\partial \rho_b}{\partial P_w} + \rho_b \frac{\partial s}{\partial P_w}\right]^{-1} \tag{8}$$

where $\partial(\rho_w q)/\partial z$ is solved using the finite difference approximation (see Appendix A) and the other terms are derived in the following sections.

2.2.2 Hydraulic properties

The hydraulic properties required to solve Eq.(1) are defined by the van Genuchten functions, as follows (van Genuchten, 1980):

The effective saturation, S_e [-], is defined by

$$S_e = (1 + |\alpha\psi|^n)^{-m}, \quad \psi < 0 \tag{9}$$

$$S_e = 1, \quad \psi \geq 0 \tag{10}$$

where ψ [L] is the pressure head, α [L^{-1}] is the reciprocal of a reference state pressure head, n [-] is an empirical exponent and $m = 1 - 1/n$ [-].

The hydraulic conductivity in the z-direction, K_z [LT^{-1}], is found from

$$K_z = K_s, \quad t = 0 \tag{11}$$

$$K_z = K_s {S_e}^{\eta}[1 - (1 - {S_e}^{1/m})^m]^2, \quad t > 0 \tag{12}$$

where K_s [LT^{-1}] is the saturated hydraulic conductivity and η [-] is an empirical exponent.

The rate of flow of water into the clay plug per unit area, q [LT^{-1}], is defined as follows

$$q = -K_z \frac{\partial h}{\partial z} \tag{13}$$

where h [L] represents the hydraulic head, given by

$$h = \psi + z \tag{14}$$

The moisture content, θ [-], is found from

$$\theta = (\theta_s - \theta_r)S_e + \theta_r \tag{15}$$

where θ_s [-] and θ_r [-] represent the saturated and residual moisture content respectively.

The change in moisture content with water pressure is found by differentiating Eq.(15), yielding

$$d\theta = (\theta_s - \theta_r)dS_e + S_e(d\theta_s - d\theta_r) + d\theta_r \tag{16}$$

By assuming that θ_r represents the saturated smallest pores and θ_s represents all saturated pores, it can be said that the change in moisture content is equal in both cases and therefore $d\theta_s = d\theta_r$. It follows that

$$d\theta = (\theta_s - \theta_r)dS_e + d\theta_s \tag{17}$$

Differentiating with respect to P_w yields

$$\frac{\partial\theta}{\partial P_w} = (\theta_s - \theta_r)\frac{\partial S_e}{\partial P_w} + \frac{\partial\theta_s}{\partial P_w} \tag{18}$$

where $\partial\theta_s/\partial P_w$ is derived in Section 2.2.9 and $\partial S_e/\partial P_w$ is found using the chain rule, as follows

$$\frac{\partial S_e}{\partial P_w} = \frac{\partial S_e}{\partial\psi}\frac{\partial\psi}{\partial P_w} \tag{19}$$

where $\partial S_e/\partial\psi$ is found by differentiating Eq.(9) with respect to ψ to give

$$\frac{dS_e}{d\psi} = mn|\alpha|^n|\psi|^{(n-1)}(1 + |\alpha\psi|^n)^{-(m+1)}, \quad \psi < 0 \tag{20}$$

$$\frac{dS_e}{d\psi} = 0, \quad \psi \geq 0 \tag{21}$$

Pressure head, ψ, is related to P_w as follows

$$\psi = \frac{P_w}{\rho_w g} \tag{22}$$

where g [LT^{-}2] represents the gravitational acceleration and where $P_w = P_a - P_c$ and P_c [ML^{-1}T^{-2}] represents the capillary pressure. It has been assumed that air is inviscid and therefore air pressure, P_a [ML^{-1}T^{-2}], is at atmospheric level, i.e. $P_a = 0$.

Differentiating Eq.(22) with respect to P_w leads to

$$\frac{\partial \psi}{\partial P_w} = \psi \left[\frac{1}{P_w} - C_F \right] \tag{23}$$

where C_F [M^{-1}LT^{2}] represents the fluid compressibility.

2.2.3 The Langmuir adsorption isotherm

Sorbed water is represented by a Langmuir adsorption isotherm. Adsorption isotherms describe the process whereby a substance in the aqueous phase, the adsorbate, is retained or released by the solid phase, the adsorbent (Foo & Hameed, 2010). In the case of the clay swelling system, the clay mineral is the adsorbent and water migrating through the plug is the adsorbate. Following the approach taken by various coalbed methane desorption models (e.g. Levine (1996), Palmer & Mansoori (1998)), this model employs the use of the Langmuir adsorption isotherm to represent the adsorption of water by the clay. The Langmuir isotherm makes a number of assumptions which can be adequately applied to the clay swelling system. It is assumed that there is a limit to the adsorption capacity of the clay and that the system undergoes monolayer adsorption, i.e. one molecule of water is sorbed at each adsorption site (Limousin et al., 2007; Foo & Hameed, 2010). This means that once all sites are filled the maximum adsorption capacity has been reached and no more adsorption occurs (Foo & Hameed, 2010). It

is also assumed that temperature is constant and all adsorption sites are identical and homogeneous, i.e. no one site has a greater affinity for the adsorbate than any other site (Limousin et al., 2007; Foo & Hameed, 2010). The Langmuir isotherm is derived according to Limousin et al. (2007), as follows:

Consider the following chemical reaction (Limousin et al., 2007)

$$\text{solute} + \text{free site} \rightleftharpoons \text{adsorbed complex} \tag{24}$$

In the clay swelling system the solute represents pore-water and the free site represents the clay mineral surface.

The equilibrium constant for this system, K_e [$\mathrm{M}^{-1}\mathrm{L}^3$], represents the affinity of the water for the clay surface (Limousin et al., 2007) and can be defined as follows

$$K_e = \frac{[\text{adsorbed complex}]}{[\text{solute}][\text{free site}]} = \frac{[X]}{[C][F]} \tag{25}$$

where $[X]$ [ML^{-3}] represents the concentration of the adsorbed complex, $[C]$ [ML^{-3}] represents the concentration of the solute, and $[F]$ [ML^{-3}] represents the concentration of the free site (i.e. the adsorbent), where $F = X_{max} - X$, and X_{max} represents the maximum adsorption capacity.

Rearranging Eq.(25) leads to the general form of the Langmuir isotherm, defined by

$$\frac{X}{X_{max}} = \frac{K_e C}{1 + K_e C} \tag{26}$$

The system reaches equilibrium when $X = X_{max}$ (Limousin et al., 2007; Foo & Hameed, 2010).

2.2.4 Parameterisation of the Langmuir isotherm for a clay swelling system

Let s [-] represent the mass of water sorbed per unit mass of clay matrix, s_{max} [-] represent the maximum adsorption capacity and c [$\mathrm{ML^{-3}}$] represent the mass of pore-water per unit volume of pore-space, such that Eq.(26) becomes

$$\frac{s}{s_{max}} = \frac{K_d c}{s_{max} + K_d c} \tag{27}$$

where $K_d = K_e s_{max}$ [$\mathrm{M^{-1}L^3}$] and represents the linear isotherm partition coefficient.

The maximum adsorption capacity, s_{max} [-], is defined by

$$s_{max} = \frac{\rho_w \theta_s s_F}{\rho_b} \tag{28}$$

where s_F [-] describes how much water is adsorbed as a multiple of the maximum mass of water that can be stored in the pore-space. When $s_F = 0$ no sorption takes place and all water is contained within the pore-space.

The mass of water in the pore-space per unit volume of clay, c [$\mathrm{ML^{-3}}$], is found from

$$c = \frac{\rho_w \theta}{\theta_s} \tag{29}$$

At small values of c, K_d represents the initial gradient of the isotherm (Limousin et al., 2007), and can therefore be defined as follows

$$K_d = \frac{s}{c} = \frac{s\theta_s}{\rho_w \theta} \tag{30}$$

At the point when $s = s_{max}$, $S_e = S_{ef}$, such that Eq.(30) becomes

$$K_d = \frac{s_{max}\theta_s}{\rho_w[(\theta_s - \theta_r)S_{ef} + \theta_r]} \tag{31}$$

where S_{ef} [-] is the fraction of S_e where maximum adsorption has almost occurred ($0 < S_{ef} < 1$), described by Figure 2.2.

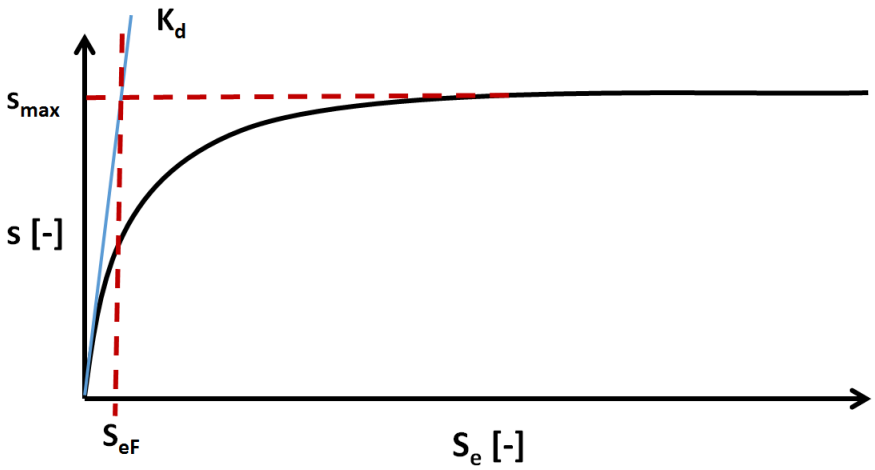

Figure 2.2: Graph to show how S_{ef} has been determined.

Using the chain rule it is possible to determine the change in mass of water sorbed with water pressure, as follows

$$\frac{\partial s}{\partial P_w} = \frac{\partial s}{\partial c}\frac{\partial c}{\partial P_w} \tag{32}$$

where $\partial s/\partial c$ is found by differentiating Eq.(27) with respect to c, yielding

$$\frac{\partial s}{\partial c} = \frac{s_{max}^2 K_d}{(s_{max} + K_d c)^2} \tag{33}$$

Differentiating Eq.(29) with respect to P_w leads to

$$\frac{\partial c}{\partial P_w} = c\left[\frac{1}{\rho_w}\frac{\partial \rho_w}{\partial P_w} + \frac{1}{\theta}\frac{\partial \theta}{\partial P_w} - \frac{1}{\theta_s}\frac{\partial \theta_s}{\partial P_w}\right] \tag{34}$$

2.2.5 Water density

Consider the following definition of fluid compressibility, C_F

$$C_F = \frac{1}{\rho_w}\frac{\partial \rho_w}{\partial P_w} \tag{35}$$

Separating the variables and integrating leads to

$$C_F \int \partial P_w = \int \frac{1}{\rho_w} \partial \rho_w \tag{36}$$

$$\ln\left(\frac{\rho_w}{\rho_{w0}}\right) = C_F(P_w - P_{w0}) \tag{37}$$

where ρ_{w0} [$\mathrm{ML^{-3}}$] and P_{w0} [$\mathrm{ML^{-1}T^{-2}}$] represent the initial water density and initial water pressure respectively.

Rearranging for ρ_w leads to

$$\rho_w = \rho_{w0} \exp[C_F(P_w - P_{w0})] \tag{38}$$

A term for $\partial \rho_w / \partial P_w$ can be derived by rearranging Eq.(35), as follows

$$\frac{\partial \rho_w}{\partial P_w} = \rho_w C_F \tag{39}$$

2.2.6 Bulk density

The bulk density of clay, ρ_b, can be defined as follows

$$\rho_b = \frac{M_b}{V_b} = \frac{M_w + M_a + M_{dc}}{V_b} \tag{40}$$

where M_b [M] represents the bulk mass, V_b [$\mathrm{L^3}$] represents the bulk volume and M_a [M]

and M_{dc} [M] represent the mass of air and dry clay matrix respectively, and can be defined further

$$M_a = V_b \rho_a (\theta_s - \theta) \tag{41}$$

$$M_{dc} = V_{dc} \rho_{dc} \tag{42}$$

where ρ_a [ML^{-3}] and ρ_{dc} [ML^{-3}] represent the density of air and dry clay matrix respectively.

The mass of water, M_w, is found from

$$M_w = M_{wp} + M_{ws} \tag{43}$$

where M_{wp} [M] represents the mass of water stored in the pore-space and M_{ws} [M] represents the mass of water sorbed by the clay. These terms are defined as follows

$$M_{wp} = \rho_w V_{wp} \tag{44}$$

$$M_{ws} = \rho_w V_{ws} \tag{45}$$

where V_{wp} [L^3] represents the volume of water stored in the pore-space and V_{ws} [L^3] represents the volume of water sorbed by the clay.

Following the definitions of θ and s it can be said that

$$M_{wp} = V_b \rho_w \theta \tag{46}$$

$$M_{ws} = V_b \rho_b s \tag{47}$$

Substituting these terms into Eq.(43) yields

$$M_w = V_b(\rho_w\theta + \rho_b s) \tag{48}$$

The bulk volume, V_b, is found from

$$V_b = V_p + V_c \tag{49}$$

where V_p [L^3] represents the volume of the pore-space and V_c [L^3] represents the volume of the wet clay matrix, which can be further defined as follows

$$V_c = V_{ws} + V_{dc} \tag{50}$$

The volume of the dry clay matrix, V_{dc}, is therefore found from

$$V_{dc} = V_b - V_p - \frac{V_b\rho_b s}{\rho_w} \tag{51}$$

It follows that

$$\rho_b = \rho_w\theta + \rho_b s + \rho_a(\theta_s - \theta) + \left(1 - \theta_s - \frac{\rho_b}{\rho_w}s\right)\rho_{dc} \tag{52}$$

where $\theta_s = \phi = V_p/V_b$ and ϕ [-] represents the porosity.

Rearranging for ρ_b leads to

$$\rho_b = \frac{\rho_w[\rho_w\theta + \rho_a(\theta_s - \theta) + \rho_{dc}(1 - \theta_s)]}{\rho_w(1 - s) + s\rho_{dc}} \tag{53}$$

In order to derive an equation for $\partial\rho_b/\partial P_w$, Eq.(53) must first be differentiated logarithmically, as follows

$$\ln(\rho_b) = \ln(\rho_w) + \ln[\rho_w\theta + \rho_a(\theta_s - \theta) + \rho_{dc}(1 - \theta_s)] - \ln[\rho_w(1 - s) + \rho_{dc}s] \tag{54}$$

$$\frac{d\rho_b}{\rho_b} = \frac{d\rho_w}{\rho_w} + \frac{dF_1}{F_1} - \frac{dF_2}{F_2} \tag{55}$$

where

$$F_1 = \rho_w\theta + \rho_a(\theta_s - \theta) + \rho_{dc}(1 - \theta_s) \tag{56}$$

$$dF_1 = \theta d\rho_w + \rho_w d\theta + \rho_a(d\theta_s - d\theta) + (\theta_s - \theta)d\rho_a + (1 - \theta_s)d\rho_{dc} - \rho_{dc}d\theta_s \tag{57}$$

$$F_2 = \rho_w(1 - s) + \rho_{dc}s \tag{58}$$

$$dF_2 = (1 - s)d\rho_w - \rho_w ds + \rho_{dc}ds + sd\rho_{dc} \tag{59}$$

Differentiating with respect to P_w leads to

$$\frac{\partial\rho_b}{\partial P_w} = \rho_b\left[\frac{1}{\rho_w}\frac{\partial\rho_w}{\partial P_w} + \frac{1}{F_1}\frac{\partial F_1}{\partial P_w} - \frac{1}{F_2}\frac{\partial F_2}{\partial P_w}\right] \tag{60}$$

where

$$\frac{\partial F_1}{\partial P_w} = \theta\frac{\partial\rho_w}{\partial P_w} + \rho_w\frac{\partial\theta}{\partial P_w} + \rho_a\left(\frac{\partial\theta_s}{\partial P_w} - \frac{\partial\theta}{\partial P_w}\right) + (\theta_s - \theta)\frac{\partial\rho_a}{\partial P_w} + (1 - \theta_s)\frac{\partial\rho_{dc}}{\partial P_w} - \rho_{dc}\frac{\partial\theta_s}{\partial P_w} \tag{61}$$

$$\frac{\partial F_2}{\partial P_w} = (1 - s)\rho_w C_F + (\rho_{dc} - \rho_w)\frac{\partial s}{\partial P_w} + \frac{\partial\rho_{dc}}{\partial P_w} \tag{62}$$

The dry clay particles in the plug are assumed to be incompressible, such that the density of dry clay, ρ_{dc}, is constant and $\partial\rho_{dc}/\partial P_w = 0$.

It has also been assumed that air is inviscid and, as such, it can be said that ρ_a and

P_a are constant, and therefore that

$$\frac{\partial P_a}{\partial P_w} = 0 \tag{63}$$

$$\frac{\partial \rho_a}{\partial P_w} = 0 \tag{64}$$

2.2.7 Adaptation of the theory of linear poroelasticity

Poroelasticity describes the coupling between the hydrological and mechanical behaviour of a porous system (Jaeger et al., 2007, p.168). The Earth's crust is highly heterogeneous, comprised of fluid-saturated pores and cracks which can significantly impact the mechanical behaviour of subsurface rocks (Jaeger et al., 2007, p.168; Guéguen & Boutéca, 2004, p.ix). Changes in the pore volume of a rock due to fluid flow can induce macroscopic deformation (Jaeger et al., 2007, p.168; Guéguen & Boutéca, 2004, p.ix). Conversely, deformation, for example due to drilling operations, can lead to changes in pore volume and fluid flow (Jaeger et al., 2007, p.168; Guéguen & Boutéca, 2004, p.ix). Therefore, it can be said that the hydrological and mechanical components of the system are coupled (Jaeger et al., 2007, p.168).

Consider the following stress-strain relationship for a poroelastic and thermoelastic medium

$$\boldsymbol{\varepsilon} = \frac{1}{2G}\boldsymbol{\tau} - \frac{\nu}{2G(1+\nu)}\text{trace}(\boldsymbol{\tau})\boldsymbol{I} - \left(\frac{C_{bp}}{3}P_p + \beta\vartheta\right)\boldsymbol{I} \tag{65}$$

where $\boldsymbol{\tau}$ and $\boldsymbol{\varepsilon}$ represent the stress and strain tensors, G [$\text{ML}^{-1}\text{T}^{-2}$] represents the shear modulus, ν [-] represents Poisson's ratio, ϑ [K] represents an incremental temperature increase, β [K^{-1}] represents the linear thermal expansion coefficient and C_{bp} [M^{-1}LT^2]

represents the bulk pore compressibility and relates bulk strain, ε_b [-], to pore-pressure, P_p [$\mathrm{ML^{-1}T^{-2}}$], as follows (Jaeger et al., 2007, p.170)

$$C_{bp} = -\left(\frac{\partial \varepsilon_b}{\partial P_p}\right)_P \tag{66}$$

Taking the trace of both sides of Eq.(65) yields

$$\varepsilon_b = \frac{\tau_m}{K} - (C_{bp}P_p + 3\beta\vartheta) \tag{67}$$

where τ_m [$\mathrm{ML^{-1}T^{-2}}$] represents the trace of the stress tensor and K [$\mathrm{ML^{-1}T^{-2}}$] represents the bulk modulus.

Rewriting the stress-strain relationship for stress in terms of strain leads to

$$\boldsymbol{\tau'} = \boldsymbol{\tau} - (\alpha_B P_p + \gamma\vartheta)\boldsymbol{I} = 2G\boldsymbol{\varepsilon} + \lambda \mathrm{trace}(\boldsymbol{\varepsilon})\boldsymbol{I} \tag{68}$$

where $\boldsymbol{\tau'}$ represents the effective stress tensor, $\alpha_B = C_{bp}K$ [-] and represents the Biot coefficient and $\gamma = 3K\beta$.

2.2.8 Uniaxial strain assumption

This model simulates the migration of water through a one-dimensional clay plug, following the method applied by the Layered Mineral Geochemistry Group at Durham University in their linear swelling experiments. In order to account for this, the swelling model adopts the state of uniaxial strain. Uniaxial strain assumes that only vertical strain occurs, and that lateral strains are zero (Jaeger et al., 2007, p.112).

The uniaxial strain assumption states that $\varepsilon_{xx} = \varepsilon_{yy} = 0$ (Jaeger et al., 2007, p.112). Therefore, from Eq.(68) it is possible to determine the effective stress, τ', in each orthogonal direction (Jaeger et al., 2007, p.112)

$$\tau'_{xx} = \tau'_{yy} = \lambda \varepsilon_{zz} \tag{69}$$

$$\tau'_{zz} = (2G + \lambda)\varepsilon_{zz} \tag{70}$$

where λ [$\mathrm{ML^{-1}T^{-2}}$] represents the Lamé coefficient.

Rearranging Eq.(70) for ε_{zz} leads to

$$\varepsilon_{zz} = \frac{\tau'_{zz}}{(2G + \lambda)} \tag{71}$$

The mean effective stress, τ'_m, is defined by (Jaeger et al., 2007, p.101)

$$\tau'_m = \frac{1}{3}(\tau'_{xx} + \tau'_{yy} + \tau'_{zz}) \tag{72}$$

Therefore, it follows that

$$\tau'_m = \frac{1}{3}\left(\frac{2G + 3\lambda}{2G + \lambda}\right)\tau'_{zz} \tag{73}$$

The Lamé parameters, G and λ, are defined as follows (Jaeger et al., 2007, p.108)

$$G = \frac{E}{2(1+\nu)}, \quad \lambda = \frac{E\nu}{(1+\nu)(1-2\nu)} \tag{74}$$

where E [$\mathrm{ML^{-1}T^{-2}}$] and ν [-] represent the Young's Modulus and Poissons' ratio respectively.

Substituting the Lamé parameters into Eq.(73) leads to

$$\tau'_m = \frac{1}{3}\left(\frac{1+\nu}{1-\nu}\right)\tau'_{zz} \tag{75}$$

Palmer & Mansoori (1998) have defined a constrained axial modulus, M, related to the bulk modulus, K, as follows

$$M = \frac{3K(1-\nu)}{(1+\nu)} \tag{76}$$

It can therefore be said that

$$\tau'_m = \frac{K}{M}\tau'_{zz} \tag{77}$$

From Eq.(68)

$$\tau'_m = \tau_m - (\alpha_B P_p + 3K\beta\vartheta) \tag{78}$$

Rearranging and substituting into Eq.(77) leads to

$$\tau_m = \frac{K}{M}\tau'_{zz} + \alpha_B P_p + 3K\beta\vartheta \tag{79}$$

Substituting Eq.(79) into Eq.(67) yields

$$\varepsilon_b = \frac{\tau'_{zz}}{M} \tag{80}$$

where

$$\tau'_{zz} = \tau_{zz} - \alpha P_p - 3K\beta\vartheta \tag{81}$$

Substituting the swelling term for the thermoelastic term, where $\varepsilon_s = -3\beta\vartheta$, gives

$$\tau'_{zz} = \tau_{zz} - \alpha P_p + K\varepsilon_s \tag{82}$$

$$\varepsilon_b = \frac{1}{M}(\tau_{zz} - \alpha_B P_p + K\varepsilon_s) \tag{83}$$

2.2.9 Saturated moisture content

It has been assumed that the saturated moisture content, θ_s, represents all pores and is therefore analogous to the porosity, ϕ, of the clay plug. The equation for θ_s in this section will first be derived in terms of ϕ before substituting for θ_s.

Recall that the bulk volume, V_b, of a porous medium is defined by

$$V_b = V_p + V_c \tag{84}$$

Porosity, ϕ, is found from (Jaeger et al., 2007, p.169)

$$\phi = \frac{V_p}{V_b} = 1 - \frac{V_c}{V_b} \tag{85}$$

Differentiating Eq.(85) and re-writing in terms of strain leads to

$$-d\phi = (1 - \phi)(d\varepsilon_b - d\varepsilon_c) \tag{86}$$

where ε_c [-] represents the strain of the clay matrix.

The change in bulk strain, $d\varepsilon_b$, is found by differentiating Eq.(67), yielding

$$d\varepsilon_b = \frac{d\tau_m}{K} - C_{bp} dP_p - 3\beta d\vartheta \tag{87}$$

Partial differentiation is used to define the change in strain of the clay matrix, $d\varepsilon_c$, as follows

$$d\varepsilon_c = \left(\frac{\partial \varepsilon_c}{\partial \tau_m}\right)_{P_p,\vartheta} d\tau_m + \left(\frac{\partial \varepsilon_c}{\partial P_p}\right)_{\tau_m,\vartheta} dP_p + \left(\frac{\partial \varepsilon_c}{\partial \vartheta}\right)_{\tau_m,P_p} d\vartheta \tag{88}$$

Each of these three terms can then be found from (Jaeger et al., 2007, p.174)

$$\left(\frac{\partial \varepsilon_c}{\partial \tau_m}\right)_{P_p,\vartheta} = \frac{1}{(1-\phi)}\frac{1}{K_m} \tag{89}$$

$$\left(\frac{\partial \varepsilon_c}{\partial P_p}\right)_{\tau_m,\vartheta} = -\frac{\phi}{(1-\phi)}\frac{1}{K_m} \tag{90}$$

$$\left(\frac{\partial \varepsilon_c}{\partial \vartheta}\right)_{\tau_m,P_p} = -3\beta_m \tag{91}$$

where K_m [$\mathrm{ML^{-1}T^{-2}}$] and β_m [$\mathrm{K^{-1}}$] represent the bulk modulus and the coefficient of linear thermal expansion respectively of the clay matrix, and where K_m is found from

$$K_m = \frac{K}{1-\alpha_B} \tag{92}$$

It can therefore be said that

$$(1-\phi)d\varepsilon_c = \frac{1}{K_m}(d\tau_m - \phi dP_p) - 3(1-\phi)\beta_m d\vartheta \tag{93}$$

Substituting Eq.(93) and Eq.(87) into Eq.(86) yields

$$-d\phi = (1-\phi)\left[\frac{d\tau_m}{K} - C_{bp}dP_p - 3(\beta-\beta_m)d\vartheta\right] - \frac{1}{K_m}(d\tau_m - \phi dP_p) \tag{94}$$

Differentiating Eq.(79) and substituting into Eq.(94) leads to

$$d\phi = \frac{1}{K_m}\left(\frac{K}{M}d\tau'_{zz} + (\alpha_B - \phi)dP_p + 3K\beta d\vartheta\right) - (1-\phi)\left[\frac{1}{M}d\tau'_{zz} + 3\beta_m d\vartheta\right] \tag{95}$$

Differentiating Eq.(81) and substituting into Eq.(95) yields

$$d\phi = \frac{1}{K_m}\left(\frac{K}{M}d\tau_{zz} - \frac{K\alpha}{M}dP_p - \frac{3K^2\beta}{M}d\vartheta + (\alpha_B - \phi)dP_p + 3K\beta d\vartheta\right) \\ -(1-\phi)\left[\frac{1}{M}d\tau_{zz} - \frac{\alpha_B}{M}dP_p - \frac{3K\beta}{M}d\vartheta + 3\beta_m d\vartheta\right] \tag{96}$$

Consider the special case when $\beta = \beta_m$, such that rearranging Eq.(96) leads to

$$d\phi = (\alpha_B - \phi)\left(\frac{1}{K_m} + \frac{\alpha_B}{M}\right)dP_p + (\alpha_B - \phi)\left(\frac{K}{M} + 1\right)3\beta d\vartheta - (\alpha_B - \phi)\frac{d\tau_{zz}}{M} \tag{97}$$

where τ_{zz} is constant and therefore $d\tau_{zz} = 0$.

Substituting the swelling term for the thermoelastic term, $d\varepsilon_s = -3\beta d\vartheta$, yields

$$\frac{d\phi}{(\alpha_B - \phi)} = \left(\frac{1}{K_m} + \frac{\alpha_B}{M}\right)dP_p - \left(\frac{K}{M} + 1\right)d\varepsilon_s \tag{98}$$

It follows that

$$\frac{1}{(\alpha_B - \phi)}\frac{\partial\phi}{\partial P_p} = \left(\frac{1}{K_m} + \frac{\alpha_B}{M}\right) - \left(\frac{K}{M} + 1\right)\frac{\partial\varepsilon_s}{\partial P_p} \tag{99}$$

Integrating Eq.(99) with respect to P_p leads to

$$\ln\left(\frac{\alpha_B - \phi_0}{\alpha_B - \phi}\right) = \left(\frac{1}{K_m} + \frac{\alpha_B}{M}\right)(P_p - P_{p0}) - \left(\frac{K}{M} + 1\right)(\varepsilon_s - \varepsilon_{s0}) \tag{100}$$

where ϕ_0 [-], P_{p0} [$\mathrm{ML^{-1}T^{-2}}$] and ε_{s0} [-] represent the initial porosity, initial pore-pressure and initial swelling strain respectively.

Rearranging for ϕ yields

$$\phi = \alpha_B - (\alpha_B - \phi_0) \exp\left[-\left(\frac{1}{K_m} + \frac{\alpha_B}{M}\right)(P_p - P_{p0}) + \left(\frac{K}{M} + 1\right)(\varepsilon_s - \varepsilon_{s0}) \right] \quad (101)$$

Recall that $\phi = \theta_s$, such that

$$\theta_s = \alpha - (\alpha_B - \theta_{s0}) \exp\left[-\left(\frac{1}{K_m} + \frac{\alpha_B}{M}\right)(P_p - P_{p0}) + \left(\frac{K}{M} + 1\right)(\varepsilon_s - \varepsilon_{s0}) \right] \quad (102)$$

Returning to Eq.(98) and rewriting in terms of θ_s, it is possible to derive a term for $\partial\theta_s/\partial P_w$. Differentiating with respect to P_w leads to

$$\frac{\partial \theta_s}{\partial P_w} = (\alpha_B - \theta_s) \left[\left(\frac{1}{K_m} + \frac{\alpha_B}{M}\right) \frac{\partial P_p}{\partial P_w} - \left(\frac{K}{M} + 1\right) \frac{\partial \varepsilon_s}{\partial P_w} \right] \quad (103)$$

where the pore pressure, P_p, is related to the water pressure, P_w, as follows

$$P_p = S_w P_w + (1 - S_w) P_a \quad (104)$$

where $P_a = 0$ and $S_w = \theta/\theta_s$ [-] and represents the water saturation.

Differentiating with respect to P_w leads to

$$\frac{\partial P_p}{\partial P_w} = S_w \quad (105)$$

The term $\partial\varepsilon_s/\partial P_w$ is defined using the chain rule

$$\frac{\partial \varepsilon_s}{\partial P_w} = \frac{\partial \varepsilon_s}{\partial s} \frac{\partial s}{\partial P_w} \quad (106)$$

where $\partial\varepsilon_s/\partial s$ is found from

$$\frac{\varepsilon_s}{\varepsilon_{s,max}} = \frac{s}{s_{max}} \tag{107}$$

$$\frac{\partial \varepsilon_s}{\partial s} = \frac{\varepsilon_{s,max}}{s_{max}} \tag{108}$$

2.2.10 Maximum swelling strain

This model assumes that swelling reaches a maximum value, $\varepsilon_{s,max}$, at which point equilibrium is reached and no further expansion takes place.

Recall that the bulk strain, ε_b, and the swelling strain, ε_s, are related by the following equation

$$\varepsilon_b = \frac{1}{M}(\tau_{zz} - \alpha_B P_p + K\varepsilon_s) \tag{109}$$

It follows that

$$\varepsilon_b - \varepsilon_{b0} = -\frac{\alpha_B}{M}(P_p - P_{p0}) + \frac{K}{M}(\varepsilon_s - \varepsilon_{s0}) \tag{110}$$

where $d\tau_{zz} = 0$.

At the point when $\varepsilon_b = \varepsilon_{b,max}$, $P_p = 0$ and $\varepsilon_s = \varepsilon_{s,max}$, such that

$$\varepsilon_{b,max} - \varepsilon_{b0} = \frac{1}{M}[\alpha_B P_{p0} + K(\varepsilon_{s,max} - \varepsilon_{s0})] \tag{111}$$

Rearranging for $\varepsilon_{s,max}$ leads to

$$\varepsilon_{s,max} = \frac{1}{K}\left[M(\varepsilon_{b,max} - \varepsilon_{b0}) - \alpha_B S_{w0} P_{w0}\right] + \varepsilon_{s0} \tag{112}$$

where S_{w0} [-] represents the initial water saturation.

It should be noted that ε_b is a volumetric strain. However, because uniaxial strain

conditions are assumed, ε_b only acts in the z-direction. Extension is also negative. Because the clay plug assumes unsaturated conditions, beyond a certain height the plug cannot be fully saturated by the action of capillary pressure alone. This means that the maximum bulk strain, $\varepsilon_{b,max}$, may not be reached throughout the entire plug. Therefore it can be said that $\varepsilon_{b,max}$ is greater than the observed maximum negative vertical strain by a factor, ε_{sF}

$$\varepsilon_{b,max} < \frac{H_I - H_{max}}{H_I} \tag{113}$$

$$\varepsilon_{b,max} = \frac{\varepsilon_{sF}(H_I - H_{max})}{H_I} \tag{114}$$

where H_I [L] is the initial height of the clay plug and H_{max} [L] is the maximum height achieved by the plug, found from swelling experiments undertaken by Erdogan (2016).

Substituting Eq.(114) into Eq.(112) leads to

$$\varepsilon_{s,max} = \frac{1}{K}\left[M\left(\frac{\varepsilon_{sF}(H_I - H_{max})}{H_I} - \varepsilon_{b0}\right) - \alpha_B S_{w0} P_{w0}\right] + \varepsilon_{s0} \tag{115}$$

For the purpose of this model it has been assumed that $\varepsilon_{b0} = \varepsilon_{s0} = 0$.

2.2.11 Mapping elevation from a non-swelling domain to a swelling domain

This model currently operates on a static grid, which means that the increase in height of the plug due to sorption is not being taken into account. To rectify this, the data points are mapped onto a domain which incorporates swelling, i.e. contains a moving grid. This has been done through the introduction of a change of variables, as follows

$$\zeta = \frac{z}{H(t)}, \quad T = t \tag{116}$$

where H [L] is the height of the clay plug.

Application of the chain rule maps the data points from the non-swelling domain to the swelling domain

$$\frac{\partial P_w}{\partial z} = \frac{\partial P_w}{\partial \zeta}\frac{\partial \zeta}{\partial z} + \frac{\partial P_w}{\partial T}\frac{\partial T}{\partial z} \tag{117}$$

$$\frac{\partial P_w}{\partial t} = \frac{\partial P_w}{\partial \zeta}\frac{\partial \zeta}{\partial t} + \frac{\partial P_w}{\partial T}\frac{\partial T}{\partial t} \tag{118}$$

where $\partial T/\partial z = 0$ because T is not a function of z, $\partial T/\partial t = 1$ and where $\partial \zeta/\partial t$ is found through logarithmic differentiation with respect to t

$$\frac{\partial \zeta}{\partial t} = -\frac{\zeta}{H}\frac{\partial H}{\partial t} \tag{119}$$

Rearranging Eq.(117) leads to

$$\frac{\partial P_w}{\partial \zeta} = H\frac{\partial P_w}{\partial z} \tag{120}$$

where $\partial P_w/\partial z$ is solved using the finite difference approximation (see Appendix A).

It follows that $\partial P_w/\partial T$ is defined by

$$\frac{\partial P_w}{\partial T} = \frac{\partial P_w}{\partial t} + \zeta\frac{\partial H}{\partial t}\frac{\partial P_w}{\partial z} \tag{121}$$

The change in height with time, $\partial H/\partial t$, is given by

$$\frac{\partial H}{\partial t} = -\int_0^H \frac{\partial \varepsilon_b}{\partial t} dz \tag{122}$$

where $\partial \varepsilon_b/\partial t$ is found by differentiating Eq.(83) with respect to time, as follows

$$\frac{\partial \varepsilon_b}{\partial t} = \frac{1}{M}\left[K\frac{\partial \varepsilon_s}{\partial P_w} - \alpha_B S_w\right]\frac{\partial P_w}{\partial t} \tag{123}$$

2.3 Numerical Solution

Eq.(1) takes the form of a nonlinear partial differential equation (PDE) and is best solved using numerical approximations rather than analytically (Celia et al., 1990; Zadeh, 2011; Varado et al., 2006). Following Goudarzi et al. (2016), a method of lines approach is adopted whereby the PDE is discretised in space using finite differences (see appendix A), resulting in a set of coupled non-linear ordinary differential equations (ODEs), which are integrated with respect to time using MATLAB's ODE solver, ODE15s (Shampine & Reichelt, 1997).

2.4 Data

The hydraulic parameters used in this model are obtained from the ROSETTA Model database, a computer program which uses pedotransfer functions based on soil texture (i.e. % sand, % silt, % clay) to estimate the hydraulic properties of a soil (Schaap et al., 2001).

The swelling model results are compared with experimental data obtained from Erdogan (2016). The experiments were carried out according to the method described in Section 1.2 and produced linear swelling curves for two clay plugs composed of illite and bentonite respectively.

3 Results & Discussion

This chapter is split up into three sections to discuss the results obtained from running three versions of the model, each making different assumptions and simplifications.

3.1 Capillary Suction Model

This version of the model only considers the migration of bulk pore water through the clay plug, i.e. it has been assumed that no water is adsorbed by the clay and therefore no expansion takes place. It has also been assumed that

$$\frac{1}{\phi}\frac{\partial \phi}{\partial P_w} = C_R \tag{124}$$

where C_R [$\mathrm{M^{-1}LT^2}$] represents rock compressibility.

Eq.(1) was solved using the method of lines approach previously described (Goudarzi et al., 2016), using parameter values given in Table 3.1 in conjunction with the ROSETTA pedotransfer function database (obtained from Schaap et al., 2001).

Parameter (unit)	Value
Water density, ρ_w (kg m^{-3})	1000
Acceleration due to gravity, g (m s^{-2})	9.81
Fluid compressibility, C_F (Pa^{-1})	4.8e-10
Rock compressibility, C_R (Pa^{-1})	1e-8
Initial height of plug, H_I (m)	0.05

Table 3.1: Capillary suction model parameters. Fluid and rock compressibility values taken from Schwartz & Zhang (2003, p.74)

Figure 3.1 shows how the moisture content of the clay plug varies with time. As water migrates through the pore-space the moisture content increases, until equilibrium is reached and no more water can enter the plug. For the height of the plug being modelled, saturated moisture content is not reached throughout the entire plug and the

moisture content decreases slightly with increasing elevation once equilibrium has been reached. This is because for the given height of the plug capillary pressure is not able to suck enough water to the top of the plug to fully saturate it.

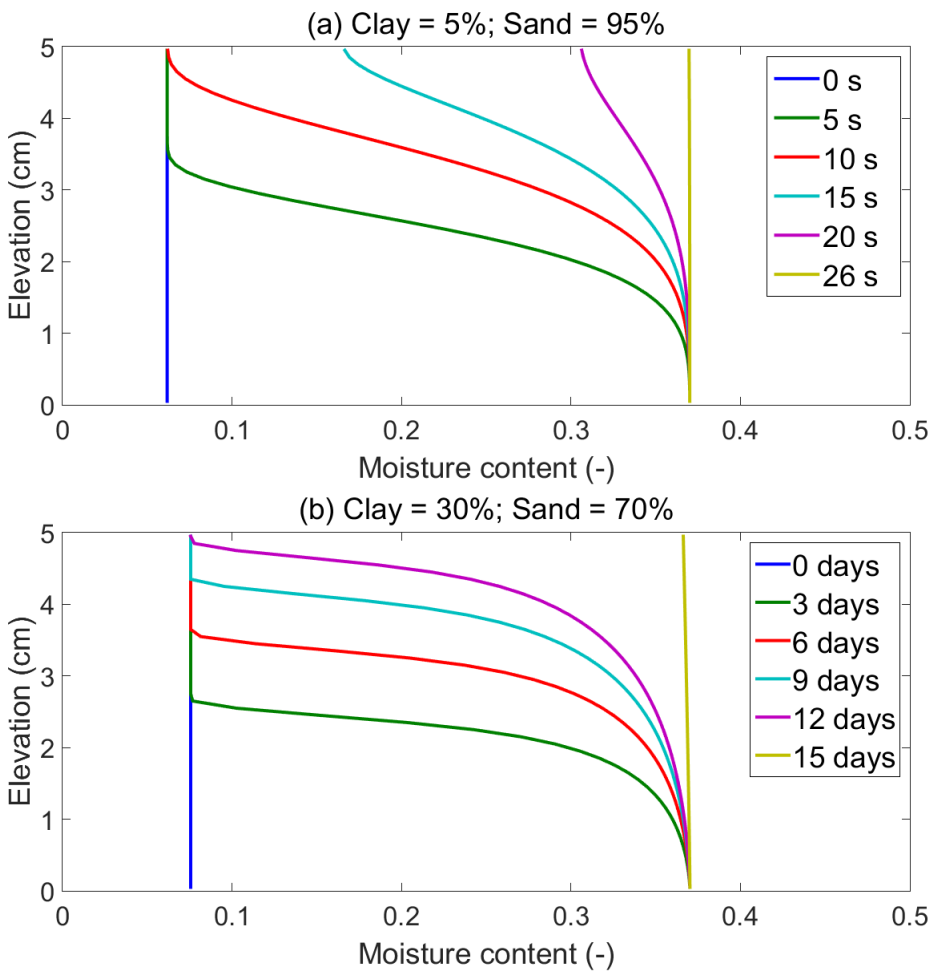

Figure 3.1: Moisture content evolution with time for plugs containing (a) 5 % clay and (b) 30 % clay. Both plugs have an initial effective saturation, S_{e0}, of 0.01. The blue and yellow lines represent the residual moisture content and the final moisture content respectively.

An increase in the clay content of the plug leads to an increase in the time taken to reach equilibrium (hereafter called the equilibrium time). As shown by Figure 3.1a, a plug containing 5 % clay takes 26 s to reach equilibrium, whereas the time taken for a

plug with a clay content of 30 % is 15 days (Figure 3.1b). This is because as clay content increases the pore-size distribution becomes less well sorted, resulting in more pores of a smaller diameter (Schwartz & Zhang, 2003, p.135). Permeability decreases with pore diameter, meaning that the rate of migration of water through the plug is reduced as clay content increases and more time is required for the plug to reach equilibrium.

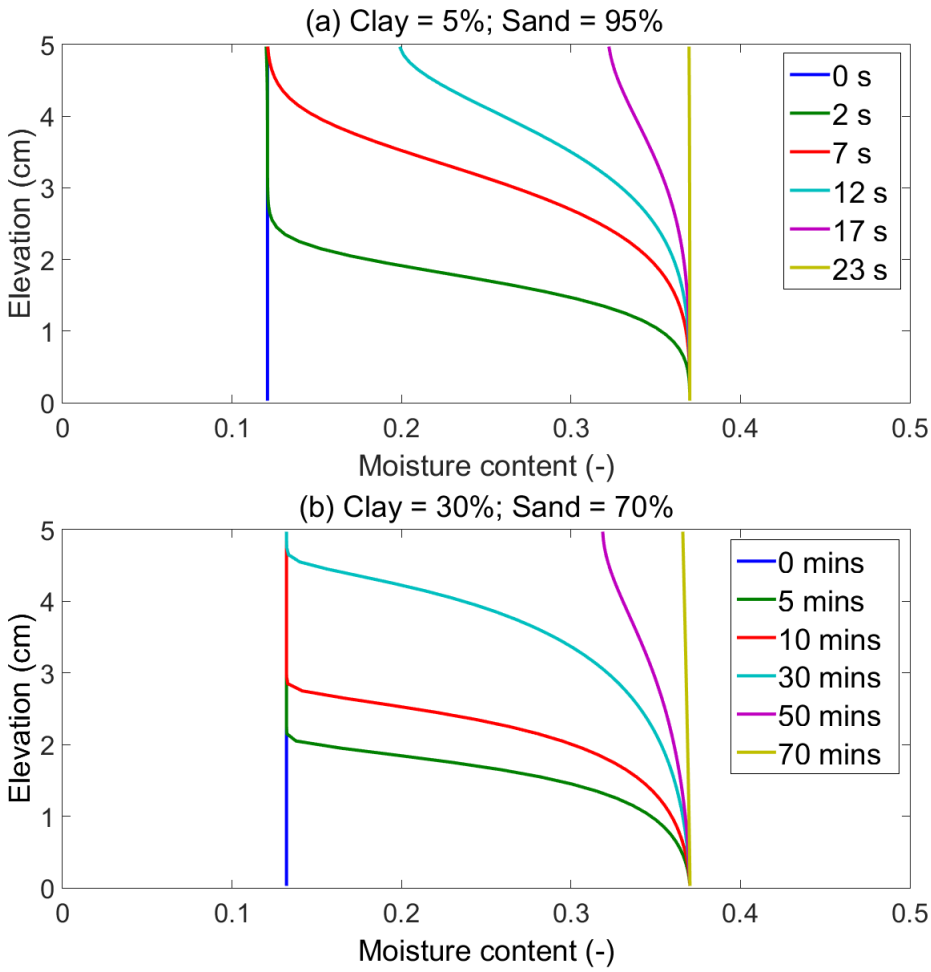

Figure 3.2: Moisture content evolution with time for plugs containing (a) 5 % clay and (b) 30 % clay. Both plugs have a S_{e0} of 0.2.

Figure 3.2 shows the evolution of moisture content with time for plugs with a higher initial effective saturation, S_{e0}. Comparison with Figure 3.1 shows that equilibrium time

decreases as initial effective saturation increases. One reason for this is because the plug contains more water initially and is therefore closer to equilibrium. Another reason is that more water in the plug results in a higher initial relative permeability throughout. For example, a plug containing 5 % clay with an initial effective saturation of 0.01, has a relative permeability of 5.105e-5, whereas the same plug with an initial effective saturation of 0.2 has a relative permeability of 0.0199. A higher relative permeability allows for easier flow through the plug and therefore less time is taken to reach equilibrium.

Due to time constraints with running the model, results could not be obtained for plugs with clay contents higher than 30 %, despite using larger time steps. The model did run for all clay contents when using fewer grid points, but it was found that accuracy of the results was significantly reduced. A possible solution to this could be to treat the rock and water as incompressible. This should be tested with further research.

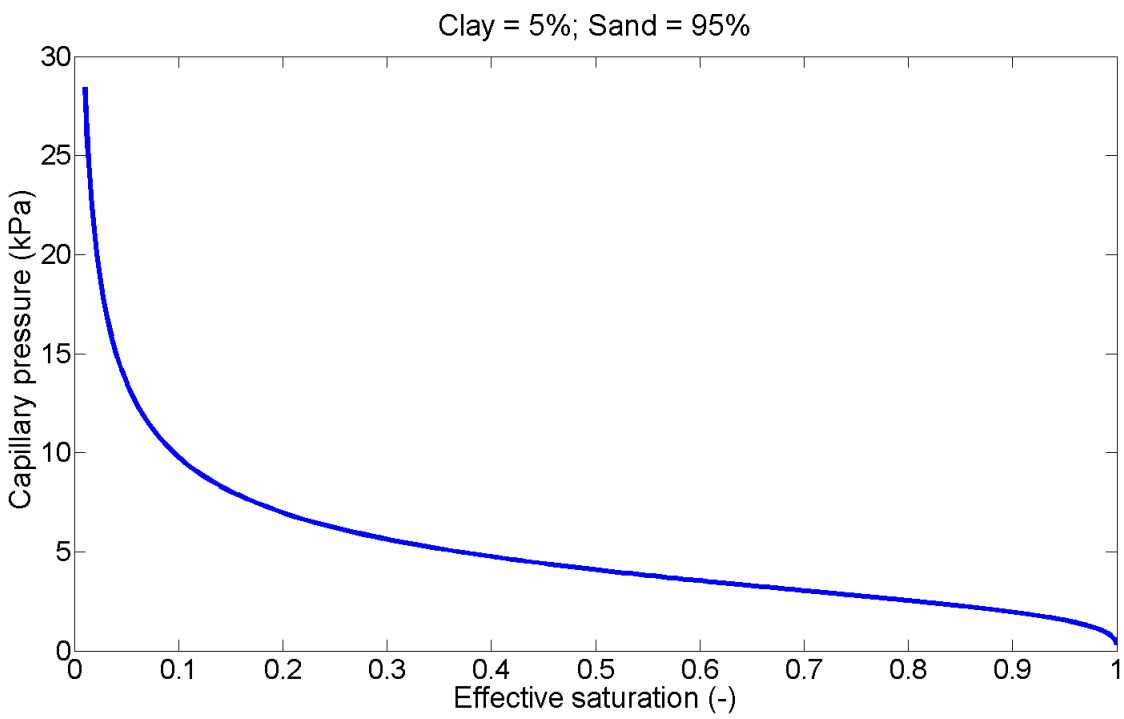

Figure 3.3: Relationship between effective saturation and capillary pressure for a plug with a clay content of 5 % and a S_{e0} of 0.01.

Capillary pressure is inversely related to effective saturation, as shown by Figure 3.3. This can be explained by considering the air entry pressure of a pore, defined as the pressure required to move water out of the pores in order for air to enter (Lu & Likos, 2004). There is an inverse relationship between pore-radius and air entry pressure (Lu & Likos, 2004). This means that air enters the largest pores first, because a lower pressure is required. Pressure needs to be increased in order for air to enter smaller pores. Figure 3.3 shows that low capillary pressure values correspond with high effective saturation values. As effective saturation decreases, i.e. water is being displaced by air, capillary pressure increases.

3.2 Sorption Model

The capillary suction model described in the previous section assumes that all water is contained within the pore-space. Here the model is extended to incorporate sorbed water through the use of the Langmuir isotherm. Swelling is not yet considered. The assumption of Eq.(124) still holds.

Eq.(1) was solved following the same approach applied to the capillary suction model, using parameter values given in Table 3.2.

Parameter (unit)	Value
Water density, ρ_w (kg m^{-3})	1000
Bulk density, ρ_b (kg m^{-3})	2600
Acceleration due to gravity, g (m s^{-2})	9.81
Fluid compressibility, C_F (Pa^{-1})	4.8e-10
Rock compressibility, C_R (Pa^{-1})	1e-8
Initial height of plug, H_I (m)	0.05

Table 3.2: Sorption model parameters. Fluid and rock compressibility values taken from Schwartz & Zhang (2003, p.74)

Figure 3.4 shows the evolution of moisture content with time for two plugs, contain-

ing 5 % and 30 % clay respectively. Comparison with Figure 3.1 shows that, following the incorporation of sorbed water, it takes longer for the plug to reach equilibrium. For example, for the plug containing 5 % clay, equilibrium time has increased from 26 s to 50 s. This is because, as water is being adsorbed by the clay mineral, it is being taken out of the pore-space and, since the rate of flow of water into the plug does not vary significantly between the two models, more water is required to migrate through the plug.

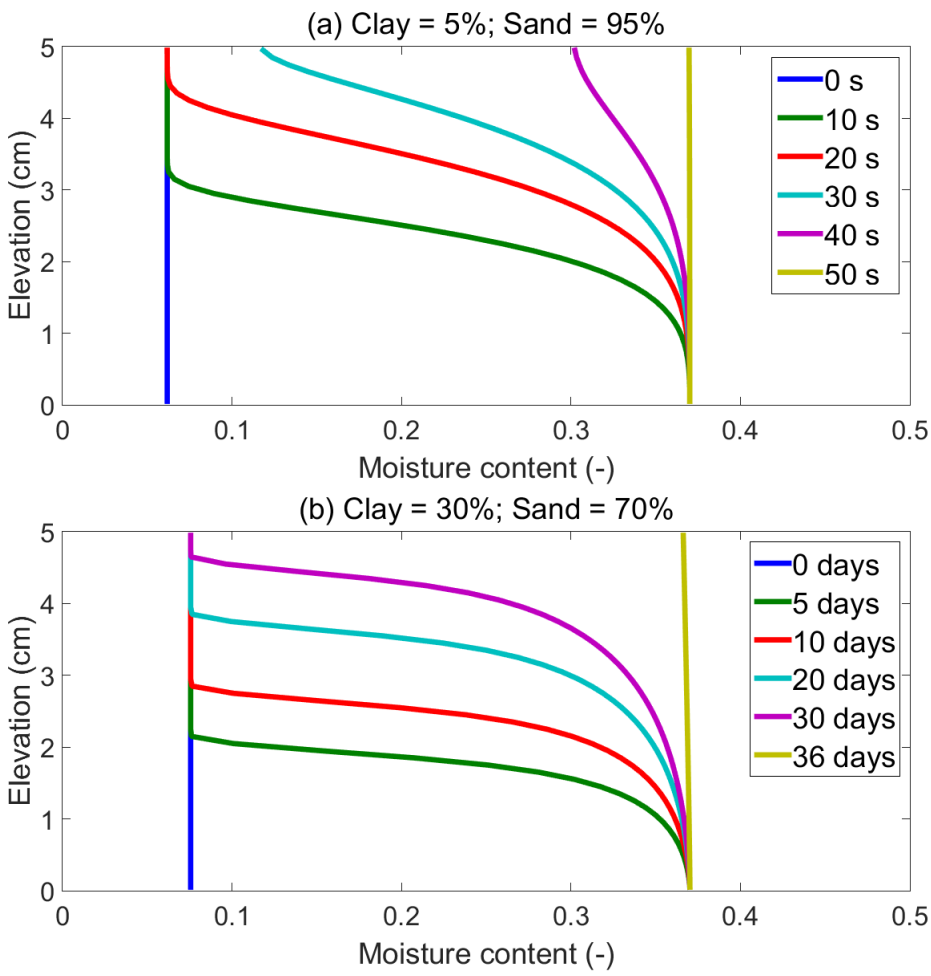

Figure 3.4: Moisture content evolution with time for plugs containing (a) 5 % clay and (b) 30 % clay. Both plugs have a S_{e0} of 0.01. The sorption parameters are $s_{maxF} = 2$ and $S_{ef} = 0.5$.

3.2.1 Sensitivity Analysis

A sensitivity analysis has been performed to determine the impact the newly defined sorption parameters, s_F and S_{ef}, have on equilibrium times for plugs of varying clay content.

Recall that s_F describes how much more water is adsorbed compared with the amount in the pore-space. This suggests that as s_F is increased, time taken to reach equilibrium will increase. Figure 3.5 confirms this and indicates a linear relationship between s_F and equilibrium time. The results also show that the difference in equilibrium times produced by s_F values of 1 and 10 increases with clay content, indicating that s_F has more influence on equilibrium time as clay content increases. Additionally it is shown that when $s_F = 0$ the sorption model replicates the capillary suction model.

Higher values of s_F were tested ($s_F = 15, 25, 50$) and followed the same trend.

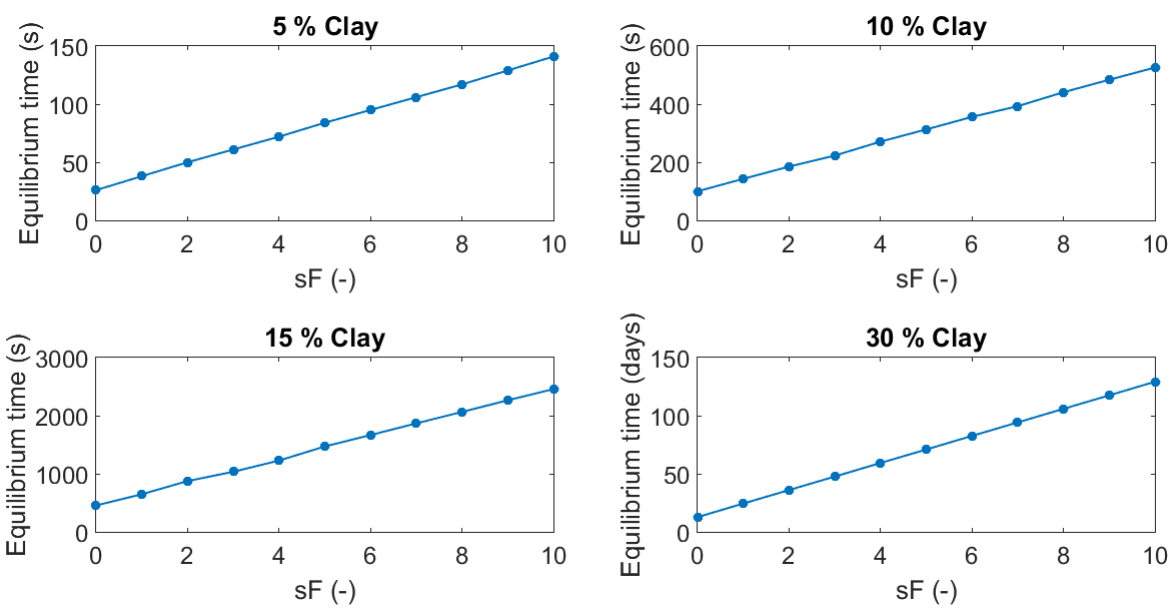

Figure 3.5: Variation of equilibrium time with s_F for four plugs with different clay contents. Other parameters held constant: $S_{e0} = 0.01$, $S_{ef} = 0.5$. Note that when $s_F = 0$ no water is sorbed and the sorption model replicates the capillary suction model.

Figure 3.6 shows how equilibrium time varies with S_{ef}. For plugs containing 5 %, 10 % and 15 % clay, figure 3.6 shows that as S_{ef} is increased, equilibrium time increases initially, before decreasing again once $S_{ef} = 0.4$. As clay content of the plug increases, the range of equilibrium times also increases, suggesting that S_{ef} has a greater impact on equilibrium time for plugs containing more clay. The plug with a clay content of 30 % does not show an initial increase in equilibrium time, only a decrease. The definition of S_{ef} suggests that as S_{ef} increases, equilibrium time decreases, as is shown by all four plugs. It is not currently known why the initial increase in equilibrium time occurs, but it appears to disappear once clay content of the plug reaches 30 %.

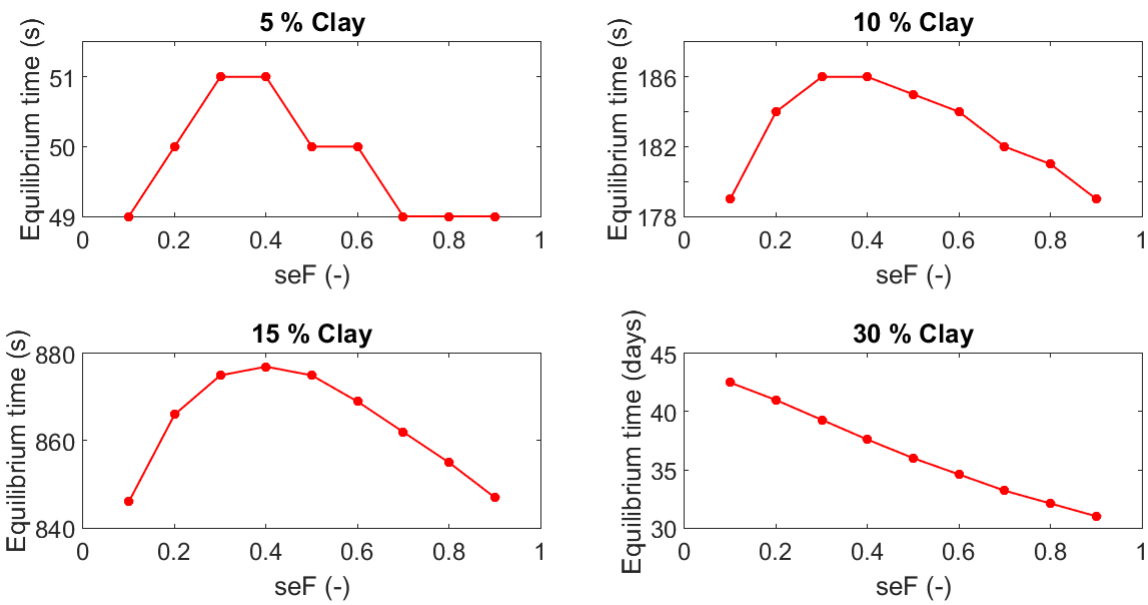

Figure 3.6: Variation of equilibrium time with S_{ef} for four plugs with different clay contents. Other parameters held constant: $S_{e0} = 0.01$, $s_F = 2$.

3.3 Swelling Model

This model incorporates expansion due to sorption of water, assuming uniaxial strain conditions and that the height of the clay plug is a function of time.

Eq.(121) was also solved by following the same approach used in the capillary suction and sorption models, using parameter values given in Table 3.3.

Parameter (unit)	Value
Initial water density, ρ_{w0} (kg m^{-3})	1000
Initial bulk density, ρ_{b0} (kg m^{-3})	2600
Dry clay density, ρ_{dc} (kg m^{-3})	1600
Air density, ρ_a (kg m^{-3})	1.225
Acceleration due to gravity, g (m s^{-2})	9.81
Fluid compressibility, C_F (Pa^{-1})	4.8e-10
Initial height of plug, H_I (m)	0.05
Bulk modulus, K (Pa)	4.9e9
Poisson's ratio, ν (-)	0.15
Biot coefficient, α_B (-)	1

Table 3.3: Swelling model parameters. Bulk modulus, Poisson's ratio and Biot coefficient are for the Boise sandstone, taken from Jaeger et al., (2007, p.190). Fluid compressibility value taken from Schwartz & Zhang (2003, p.74)

Figure 3.7a shows the moisture content evolution of a swelling plug with a clay content of 5 %. The equilibrium time has increased compared with the sorption and capillary suction model results. This is because the plug has been allowed to grow and more water is required to fill the larger volume. Since the rate of flow of water into the plug does not vary significantly between the models, more time is required for water to migrate to the top of the plug.

Figure 3.7b shows how the plug has swelled with time. Linear swelling is calculated as follows

$$\text{Linear swelling} = \frac{H - H_I}{H_I} \tag{125}$$

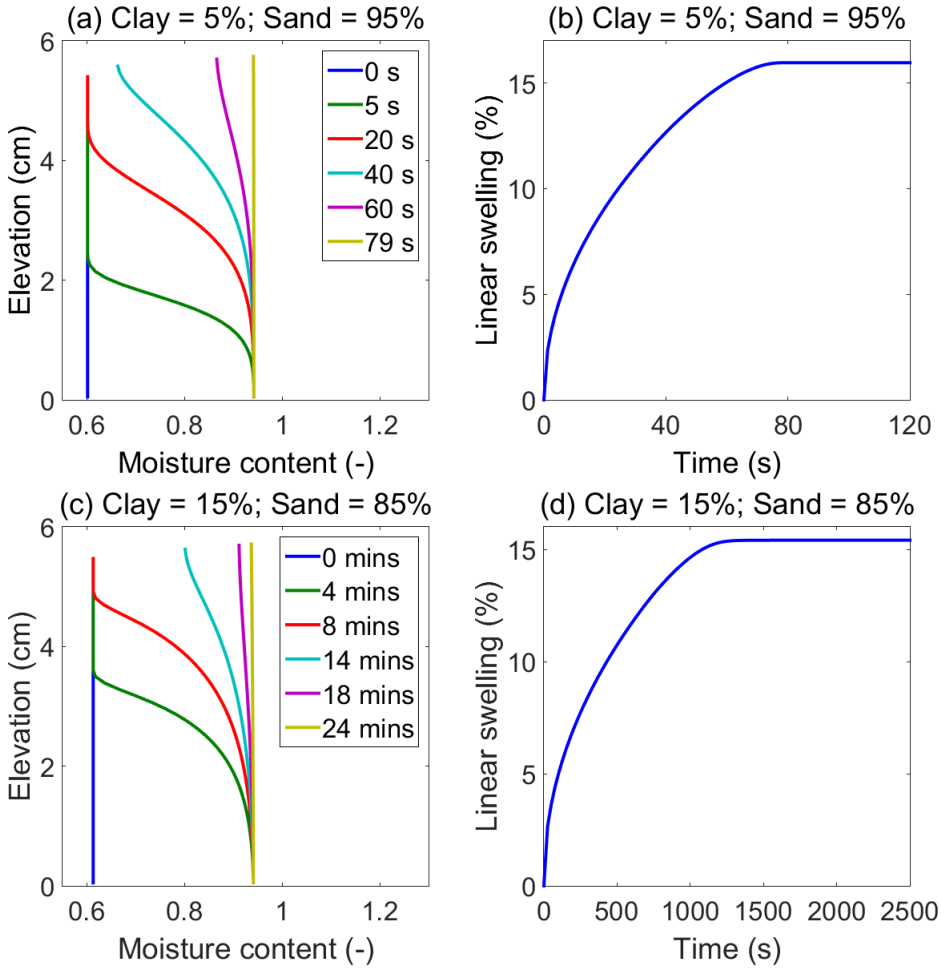

Figure 3.7: Moisture content evolution with time for plugs containing (a) 5 % clay and (c) 15 % clay. Swelling curves for plugs containing (b) 5 % clay and 15 % clay. Parameters held constant: $S_{e0} = 0.01$, $s_F = 2$, $S_{ef} = 0.5$ and $\varepsilon_{sF} = 2$.

The rate of swelling decreases with time, until a maximum height is reached and swelling ends. An increase in clay content of the plug leads to the adsorption of more water and is therefore predicted to lead to an increase in swelling. Figure 3.7 contradicts this theory, instead showing a slight decrease in swelling with increasing clay content. This may be due to the fact that it has been assumed that $\varepsilon_{s0} = 0$. If there is water in the clay plug initially, then an amount of initial swelling would be expected to occur. The more water there is in the plug initially, i.e. a higher S_{e0}, the more initial swelling

there would be. So, for a drier plug, i.e. lower S_{e0}, initial swelling would be closer to 0, improving the accuracy of the results in the model. Plugs with a lower S_{e0} were modelled (Figure 3.8) and confirm this theory. For this reason, all subsequent plugs being modelled will contain a S_{e0} of 0.001. It should be noted that the model currently does not run for plugs with a clay content higher than 15 %. The reason for this is unknown and will be investigated with further research.

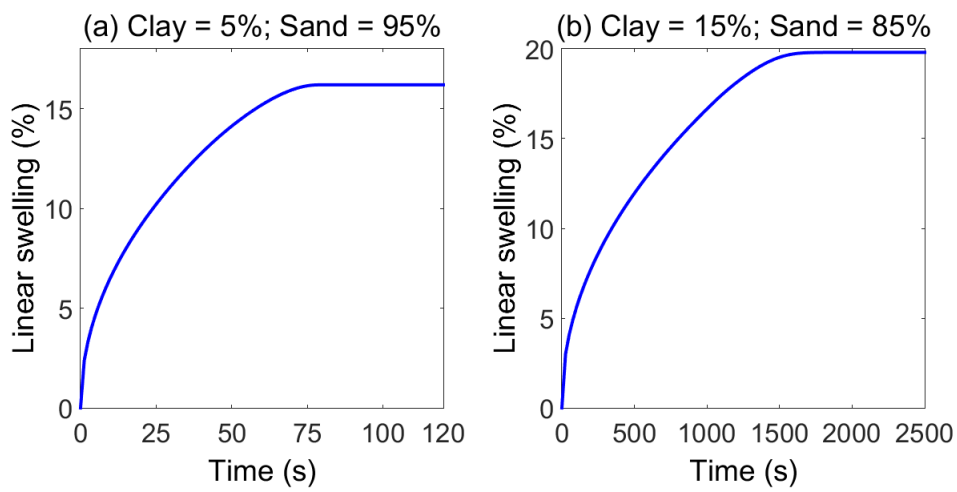

Figure 3.8: Swelling curves for plugs containing (a) 5 % clay and (b) 15 % clay with S_{e0} of 0.001.

3.3.1 Sensitivity Analysis

In addition to the sorption parameters, s_F and S_{ef}, which were defined in Section 2.2.4, another parameter is introduced: ε_{sF}. A sensitivity analysis has been performed to investigate how each parameter affects swelling for three plugs with varying clay content.

Figure 3.9 shows how varying s_F affects linear swelling for plugs containing 5 %, 10 % and 15 % clay respectively. The plugs containing 5 % and 10 % clay show the same overall trend: as s_F is increased, time taken to reach equilibrium swelling also increases,

but only up to a s_F value of 4. For higher values no change in the swelling curve is seen. This contradicts the sensitivity analysis results run on the sorption model, which show that all values of s_F between 1 and 10 impact the results. This suggests that for the swelling model s_F has become insignificant compared with overall swelling. It can also be seen that s_F has no effect on amount of swelling in these two plugs. This defies the definition of s_F which implies that an increase in s_F leads to an increase in swelling. The plug containing 15 % clay, by comparison, shows a different result. As occurs for the 5 % and 10 % clay plugs, an increase in s_F leads to an increase in the time taken to reach equilibrium swelling. However, for the 15 % clay plug s_F directly impacts the amount of swelling undergone: an increase in s_F leads to an increase in swelling. It may be that at very low clay contents s_F does not have an effect on swelling, and the effect is only seen at clay contents of 15 % or higher. This is something to investigate with further research.

The effect of using higher values of s_F has been tested (s_F = 15, 25, 50) and for the simulation of plugs containing 5 % and 10 % clay no change is seen. For the plug containing 15 % clay, swelling decreases slightly as s_F is increased, by about 0.8 %. This contradicts the definition of s_F which indicates that higher values of s_F can be used for plugs with higher clay contents, as more water is adsorbed. It is not currently known why the amount of swelling decreases with higher values of s_F for the plug containing 15 % clay, but this is something to investigate with further research.

Figure 3.10 shows how varying S_{ef} affects swelling. Simulation of all three plugs shows the same trend: an increase in S_{ef} leads to a marginal increase in swelling. For the plugs containing 5 % and 10 % clay the variation in swelling with S_{ef} is 0.9 %, but for the plug with a clay content of 15 % the variation has decreased to 0.7 %. This indicates that the variation in swelling for the range of S_{ef} values decreases with increasing clay content, thus making S_{ef} less significant as clay content increases.

However, it is difficult to investigate this thoroughly without being able to simulate plugs with higher clay content.

Figure 3.11 shows how varying ε_{sF} affects swelling for the three clay plugs. Each plug shows the same general trend: as ε_{sF} is increased amount of swelling also increases. Recall that ε_{sF} is defined as the factor by which maximum bulk strain, $\varepsilon_{b,max}$, is greater than observed maximum negative strain. An increase in ε_{sF} leads to an increase in $\varepsilon_{b,max}$ which in turn leads to an increase in $\varepsilon_{s,max}$ and therefore an increase in ε_s. The results show that this parameter has the greatest effect on overall swelling. Higher values of ε_{sF} were also tested ($\varepsilon_{sF} = 15, 25, 50$) and showed the same trend.

Overall, the sensitivity analysis shows that s_F affects the speed with which swelling takes place, and the results suggest that as clay content is increased s_F has a more significant impact on the amount of swelling, but it is difficult to make this conclusion without simulating plugs with higher clay contents. As S_{ef} is increased swelling increases by a small amount, and the results indicate that as clay content is increased, S_{ef} has a smaller impact on swelling. By comparison, ε_{sF} has the greatest impact, where an increase in ε_{sF} leads to an increase in swelling.

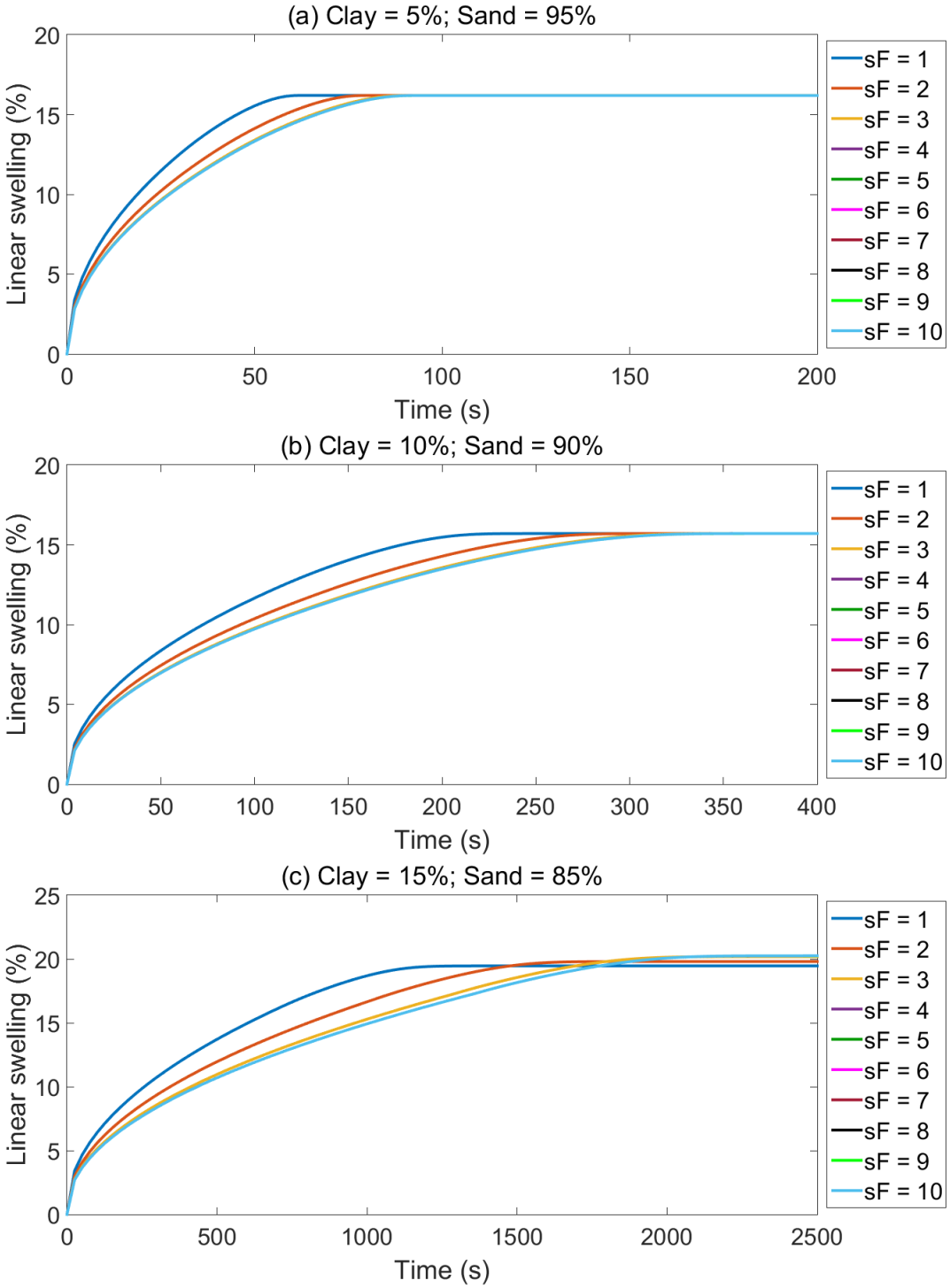

Figure 3.9: Swelling curves for varying s_F values for plugs containing (a) 5 % clay, (b) 10 % clay, (c) 15 % clay. Other parameters held constant: $S_{ef} = 0.5$, $\varepsilon_{sF} = 2$, $S_{e0} = 0.001$.

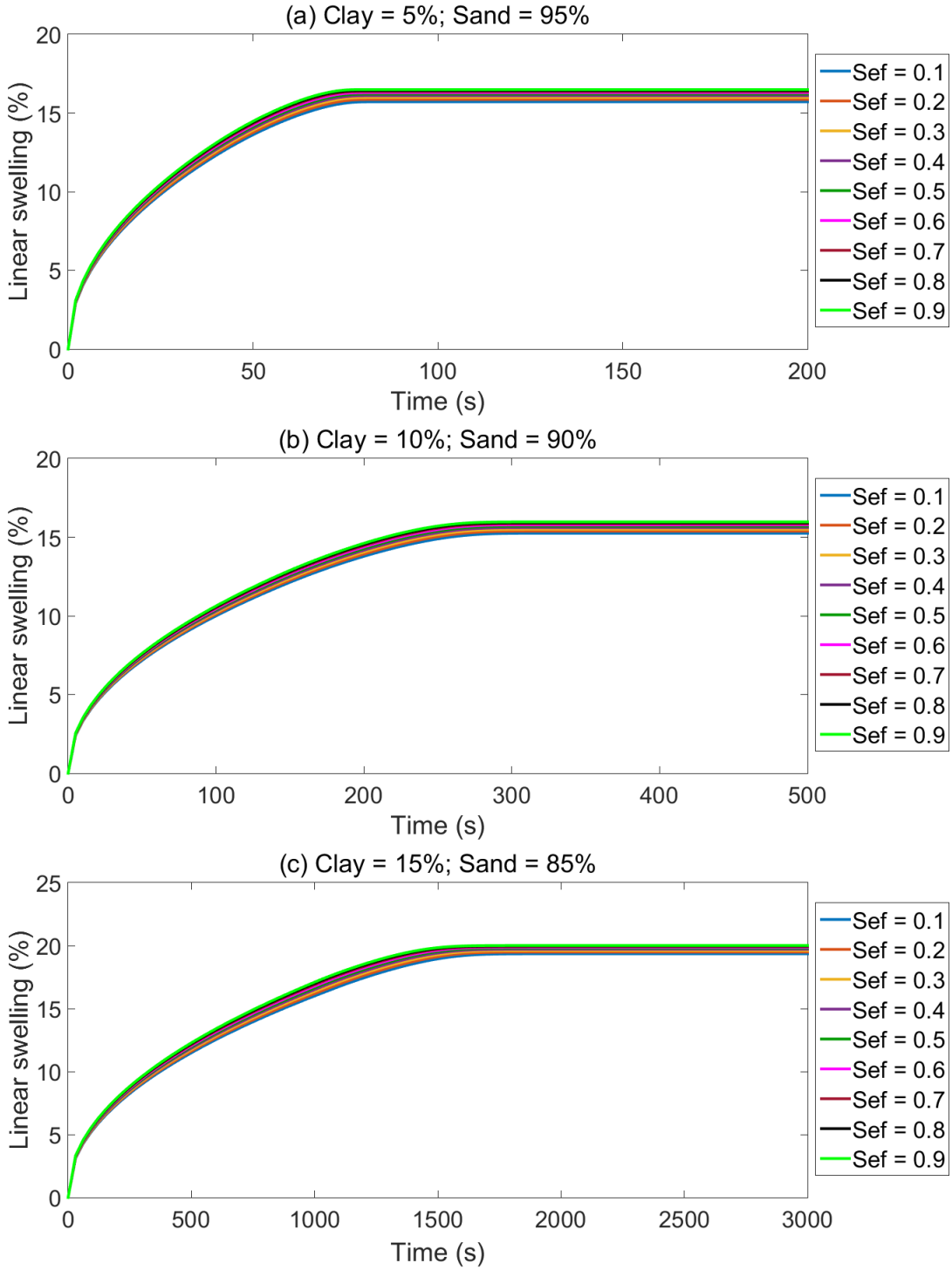

Figure 3.10: Swelling curves for varying S_{ef} values for plugs containing (a) 5 % clay, (b) 10 % clay and (c) 15 % clay. Other parameters held constant: $s_F = 2$, $\varepsilon_{sF} = 2$, $S_{e0} = 0.001$.

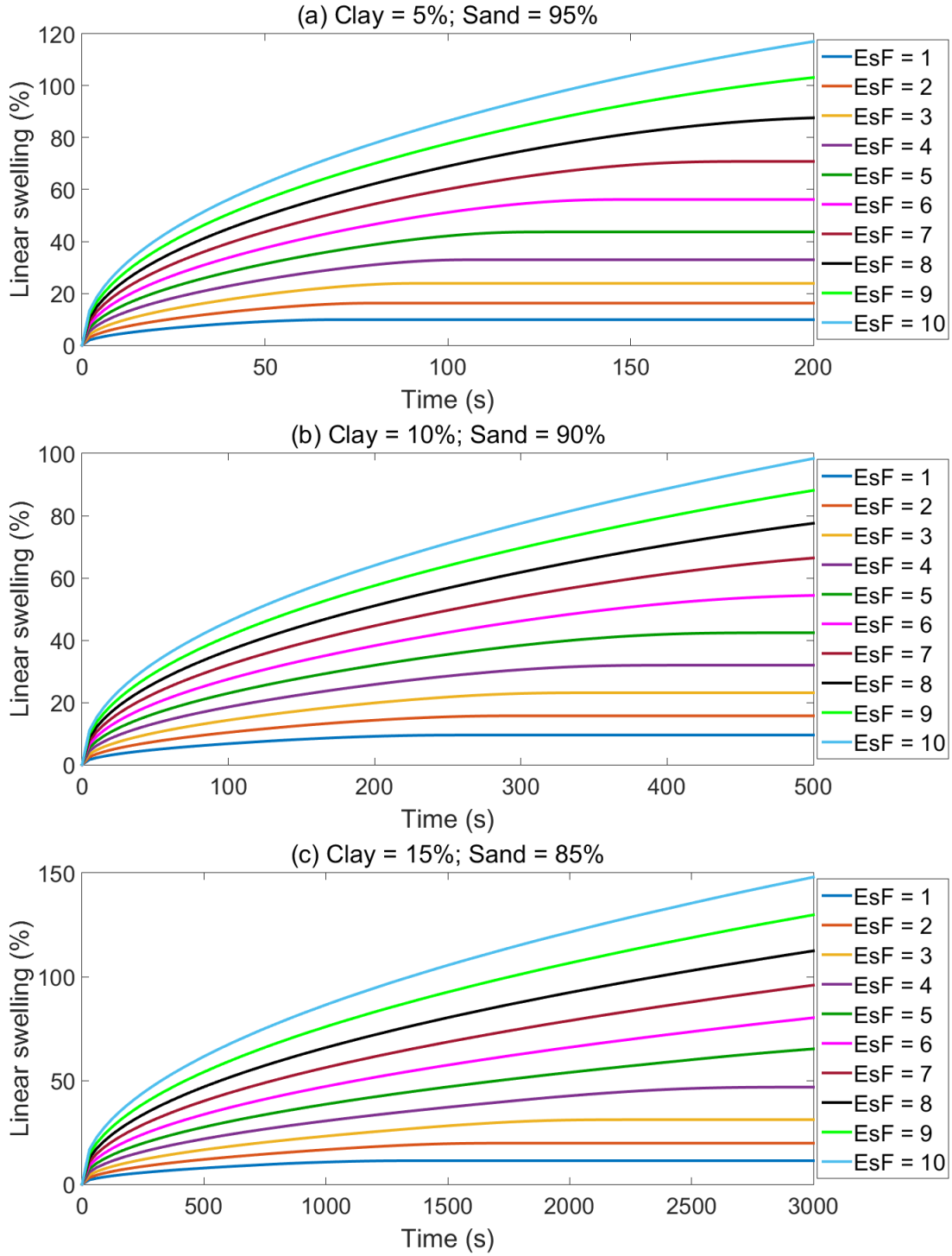

Figure 3.11: Swelling curves for varying ε_{sF} values for plugs containing (a) 5 % clay, (b) 10 % clay and (c) 15 % clay. Other parameters held constant: $s_F = 2$, $S_{ef} = 0.5$, $S_{e0} = 0.001$.

3.3.2 Comparison with Experiments

The accuracy of this swelling model has been assessed by comparing the results with those obtained from macroscopic swelling experiments undertaken by Erdogan (2016). The experimental data shows linear swelling curves for an illite and a bentonite plug which underwent expansion due to water imbibition, as has been simulated in this model. Both experimental plugs had an initial height of 0.0038 m. The model was run for three plugs containing 5 %, 10 % and 15 % clay respectively, also with an initial height of 0.0038 m. The parameters used were determined based on the results of the sensitivity analysis. It was noticed that varying the parameters had less of an effect on swelling for the smaller plug.

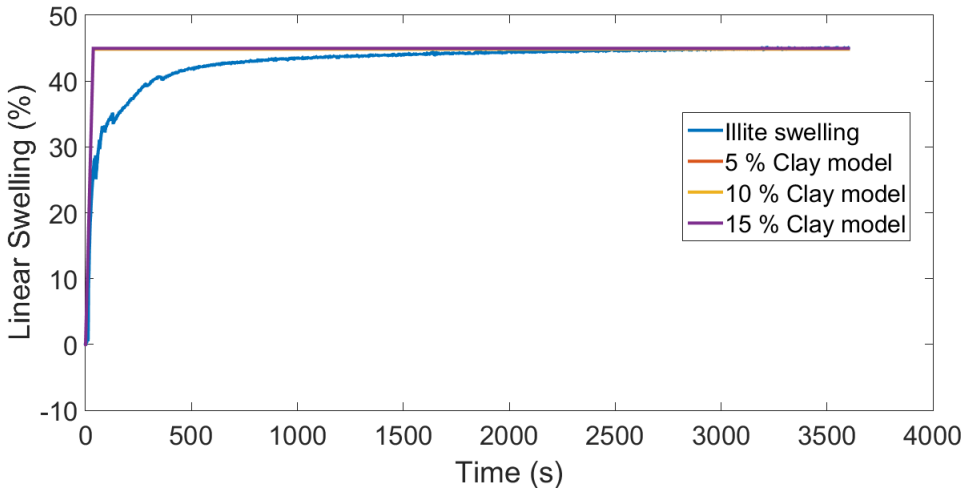

Figure 3.12: Comparison between modelled results for plugs with three different clay contents and the experimental result for an illite plug. All modelled plots overlap at this scale. Parameters used are given in Table 3.4. Data obtained from Erdogan (2016).

Figure 3.12 shows the comparison between experimental results for an illite plug and the modelled results for three clay plugs. Low values of s_F and high values of S_{ef} were used in order to fit the initial slope of the modelled plugs with the experimental result and various values of ε_{sF} were simulated in order to bring the final swelling point

as close to the illite curve as possible.

The modelled results show a significant amount of swelling over a small time period, before flattening off. Final swelling is reached after 25 seconds for all three plugs. By comparison, the illite data, whilst also showing the most swelling at the start of the experiment, curves off and swelling slows down considerably, such that final swelling is not reached until 3600 seconds have passed. The results show that it is possible for the model to achieve the same final amount of swelling as the experiment for all percentages of clay simulated. There is also a good correlation between the experimental curve and the modelled results for initial swelling. However, beyond a certain time all three modelled results diverge from the experimental curve and only converge again once the experimental plug reaches its final swelling value. The difference in shape between the modelled and experimental plots could be explained by the low clay contents of the modelled plugs (compared with the experimental plug which is composed of pure clay). A lower clay content means that final swelling is reached sooner, as is shown by Figure 3.12. There is also very little variation between the three modelled curves. This may be because small changes in clay content have less of an impact on overall swelling for a smaller plug.

Parameter (unit)	5 % Clay	10 % Clay	15% Clay
s_F (-)	1	1	1
S_{ef} (-)	0.9	0.9	0.9
ε_{sF} (-)	5.18	5.31	5.23
S_{e0} (-)	0.001	0.001	0.001
H_I (m)	0.0038	0.0038	0.0038

Table 3.4: Parameters used for comparison with illite swelling curve.

Figure 3.13 shows the comparison between experimental results for a bentonite plug and the modelled results for three clay plugs. Various values of s_F, S_{ef} and ε_{sF} were

tested to find the best fit with the experimental curve.

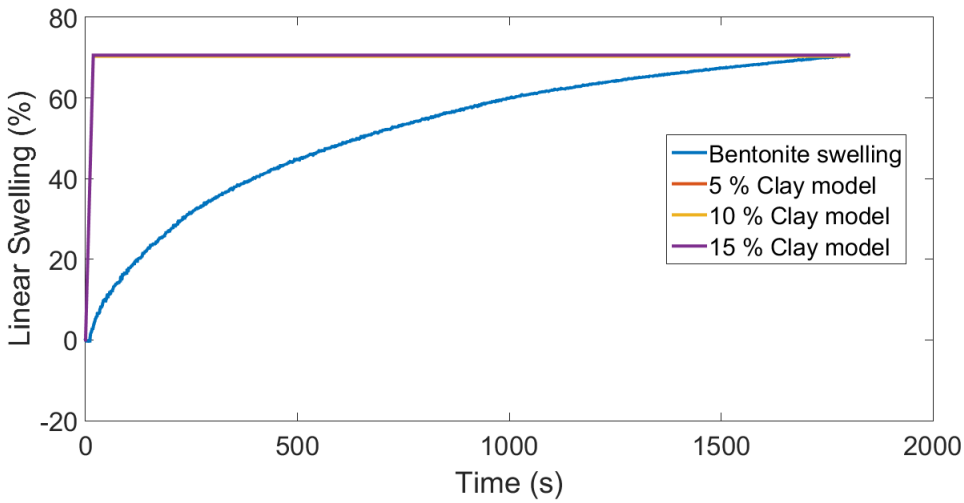

Figure 3.13: Comparison between modelled results for plugs with three different clay contents and an experimental result for a bentonite plug. Parameters used are given in Table 3.5. Data obtained from Erdogan (2016).

The results show that, as with the illite comparison, it is possible to model the same amount of swelling reached by the end of the experiment. However, in this case it is not possible to achieve good correlation for initial swelling, despite setting the most appropriate parameters. The modelled results in Figure 3.13 show a very quick increase in the height of the plug, before the plot flattens off and swelling ends. In contrast, the bentonite plug shows more gradual swelling. It has not been possible to achieve such gradual swelling with the model. A possible reason for this could be due to the low clay content of the plugs, which mean that final swelling is achieved sooner, hence the steep slopes of the modelled plugs. Given that the experimental plugs are composed of pure clay, plugs with higher clay contents need to be modelled to assess whether or not the results match with the experimental data more accurately. Another consideration is the type of clay being studied. The swelling patterns for illite and bentonite differ from each other and the modelled results show a closer resemblence to the illite plug. It

would be interesting to test the model parameters on plugs with higher clay contents to investigate whether or not the model is able to simulate both types of clay accurately.

It should be noted that the reason the amount of linear swelling does not increase with clay content in Figures 3.12 and 3.13 is because, in order to make comparisons with experimental data, the model parameters have been set to match the modelled results as accurately as possible with the experimental data, including the final amount of swelling. If the same model parameters had been used for all three modelled plugs then the amount of swelling would increase with clay content, as shown by Figure 3.8.

In conclusion, although the model was able to simulate the same amount of overall swelling as the two experimental plugs, it has not been possible to simulate the evolution of swelling with much accuracy. This indicates that the model is not suitable to simulate clay swelling at this stage. As has been discussed, further research is required to develop a model that can simulate plugs with a higher clay content to investigate whether or not convergence with experimental results improves.

Parameter (unit)	5 % Clay	10 % Clay	15 % Clay
s_F (-)	4	4	4
S_{ef} (-)	0.1	0.1	0.1
ε_{sF} (-)	7.08	7.24	7.05
S_{e0} (-)	0.001	0.001	0.001
H_I (m)	0.0038	0.0038	0.0038

Table 3.5: Parameters used for comparison with bentonite swelling curve.

4 Future Research

Comparing the results from the model with experimental results show that this model currently cannot simulate clay swelling with a high degree of accuracy. This may be partly because it is not possible to simulate the swelling of plugs containing more than 15 % clay. It is not understood why this is the case, but it is clearly a significant drawback of the swelling model and further research is required to investigate this. The inaccuracy might also be because the swelling model currently shows a mass balance error of about 8 % (difference between water entering the plug and water contained within the plug), which increases when running tests with higher ε_{sF} values. Both the capillary suction and sorption models show good mass balance, indicating that the error is associated with the swelling component of the model. Further research is required in order to determine what this error might be. Deriving a term for the initial swelling strain may also improve accuracy of the model.

Once the error in the model has been resolved and the results show good comparison with experimental data, adaptations to the model can be made to simulate borehole conditions.

One such adaptation might be to reconsider the adsorption isotherm used to represent sorption of water. The model currently uses the Langmuir isotherm because the assumptions it makes can adequately be applied to the clay swelling system. However, the Freundlich isotherm could be considered instead. This isotherm allows for multilayer adsorption rather than monolayer adsorption (Foo & Hameed, 2010), which could represent the formation of multiple hydrate layers in the interlayer region of the clay mineral.

The model currently assumes that the clay plug is physically homogeneous. In a subsurface setting this is unlikely to be the case. The model could be adapted to include

fractures or cracks in the plug to assess how fluid flow along preferential pathways affects swelling.

Drilling operations affect the in-situ stresses surrounding the borehole, resulting in pore-pressure and pore-volume changes in the surrounding rock (Jaeger et al., 2007, p.175). A way of accounting for this and therefore simulating borehole conditions more accurately could be to assume undrained compression conditions, where the confining pressure and pore-pressure are dependent on one another (Jaeger et al., 2007, p.175).

Finally, the ultimate aim of investigating the mechanisms of clay swelling is to develop effective swelling inhibitors. By varying the input parameters this swelling model could be adapted to test the impact of different fluids on the clay plug and assess which fluids are most effective at minimising swelling.

5 Conclusions

Clay swelling is a significant problem in the drilling industry and, as it is predicted that oil and gas will be important sources of energy for the foreseeable future (IEA, 2015), it is imperative to understand the mechanisms of swelling and develop effective inhibitors (Anderson et al., 2010)

This thesis develops a mathematical hydromechanical model to simulate the macroscopic swelling of clay due to water imbibition, in order to accompany macroscopic swelling experiments run by the Layered Mineral Geochemistry Group at Durham University. The sorption of water is represented by a Langmuir isotherm and a swelling strain term is derived by adapting the theory of linear poroelasticity under uniaxial strain conditions.

The results show that as the clay content of the plug is increased more time is taken for water to migrate up the plug and reach equilibrium. This is due to an increase in pore size distribution which accompanies the increase in clay content (Schwarz & Zhang, 2003). Since permeability decreases with pore diameter, the rate of migration of water through the plug is reduced and more time is taken for water to move up the plug.

It has also been shown that for a plug with a very low initial effective saturation ($S_{e0} = 0.001$) amount of swelling increases with clay content. As S_{e0} is increased, however, the opposite occurs. This could be because the initial swelling strain is assumed to be zero, which is unlikely to be the case since there is water in the plug initially. As such, it is recommended that a term for the initial swelling strain be incorporated to provide a more accurate simulation.

A sensitivity analysis of three newly defined parameters, s_F, S_{ef}, ε_{sF}, indicates that, overall, ε_{sF} has the greatest impact on swelling. The results suggest that as clay content

increases s_F has a greater impact on swelling, whereas S_{ef} has less of an impact.

A comparison with experimental swelling curves for two clay plugs shows that this swelling model is not currently able to simulate clay swelling with much accuracy. This is due to a number of limitations with the swelling model as it currently stands. First of all, the model does not run for plugs containing more than 15 % clay. Given that the experimental plugs are composed of pure clay, it is difficult to make accurate comparisons using modelled plugs containing 15 % clay or less. It might be the case that plugs with higher clay contents are able to replicate experimental results more accurately. More research is required to investigate why the model does not run for plugs with higher clay contents. The parameter s_F also needs further study. By definition, an increase in s_F should result in an increase in swelling. However, it was found that for the 15 % clay plug, swelling decreases slightly as larger values of s_F are used. The cause of this needs to be investigated further. Another limitation of the swelling model is that it currently has a mass imbalance. Although the exact cause of this imbalance is not known, it is thought to be related to the swelling component of the model, since both the capillary suction and sorption models show good mass balance. It is recommended that these errors in the model be investigated further so that this model can be used to simulate clay swelling accurately and can then be further developed to simulate in-situ clay swelling too.

6 Appendix A: Finite Difference Approximation

The terms $\partial(\rho_w q)/\partial z$ and $\partial P_w/\partial z$ have been derived using the finite difference approximation, following the approach taken by Watson et al. (2012) and Mathias et al. (2008).

The one-dimensional plug is discretised into N number of nodes along the z-axis, such that

$$0 < z_{(i)} < z_{max}, \quad i = 1...N \tag{126}$$

where $z_{(i)}$ is the value of z at the ith node and z_{max} represents z at the boundary of the plug.

It is possible to define $(\rho_w q)_{(i)}$ and $P_{w(i)}$, representing $(\rho_w q)$ and P_w at each node, which leads to the following equations

$$\frac{\partial(\rho_w q)_{(i)}}{\partial z_{(i)}} = \frac{(\rho_w q)_{(i+1/2)} - (\rho_w q)_{(i-1/2)}}{z_{(i+1/2)} - z_{(i-1/2)}} \quad i = 1...N \tag{127}$$

$$\frac{\partial P_{w(i)}}{\partial z_{(i)}} = \frac{P_{w(i+1/2)} - P_{w(i-1/2)}}{z_{(i+1/2)} - z_{(i-1/2)}} \quad i = 1...N \tag{128}$$

where boundary conditions are given by

$$q_{(i-1/4)} = K_s \left[\frac{h_{(i)} - h_0}{z_{(i)} - z_{(i-1/2)}} \right] \quad i = 1 \tag{129}$$

$$q_{(i+1/2)} = 0, \quad i = N \tag{130}$$

$$\rho_{w(i-1/2)} = \rho_{w0} \exp[-C_F P_{w0}] \tag{131}$$

$$\rho_{w(i+1/2)} = \rho_{w0} \exp[C_F (P_{w(1+1/2)} - P_{w0}] \tag{132}$$

$$P_{w(i-1/2)} = 0, \quad i = 1 \tag{133}$$

$$P_{w(i+1/2)} = \psi_{(i+1/2)}\rho_{w(i+1/2)}g \quad i = N \tag{134}$$

where, with increased grid resolution, $q_{(i-1/4)}$ tends to $q_{(i-1/2)}$.

7 Appendix B: MATLAB Codes

The MATLAB codes for the three versions of the model have been loaded onto a CD attached to the thesis.

8 Appendix C: ROSETTA Database

The ROSETTA database used in this model was obtained from Schaap et al. (2001) and can be found on the CD attached to the thesis.

9 References

Allan Freeze, R., Cherry, J.A. (1979) *Groundwater*. Prentice-Hall.

Allen, M.P. & Tildesley, D.J. (1987) *Computer simulation of liquids*. Oxford: Oxford University Press.

Amorim, C.L.G, Lopes, R.T., Barroso, R.C., Queiroz, J.C., Alves, D.B., Perez, C.A., Schelin, H.R. (2007) Effect of clay-water interactions on clay swelling by X-ray diffraction. *Nuclear Instruments and Methods in Physics Research A*. 580. p.768-770.

Anderson, R.L., Ratcliffe, I., Greenwell, H.C., Williams, P.A., Cliffe, S., Coveney, P.V. (2010) Clay swelling - A challenge in the oilfield. *Earth-Science Revies*. 98. p.201-216.

Bear, J. & Cheng, A.H.D. (2010) *Modeling groundwater flow and contaminant transport*. Netherlands: Springer Netherlands.

Bennethum, L.S. (2007) Theory of flow and deformation of swelling porous materials at the macroscale. *Computers and Geotechnics*. 34. p.267-278.

Bennethum, L.S., Cushman, J.H. (1996) Multiscale, hybrid mixture theory for swelling systems - 1: Balance laws. *International Journal of Engineering Science*. 24(2). p.125-145.

Bennethum, L.S., Cushman, J.H., Murad, M.A. (1996) Clarifying mixture theory and the macroscale chemical potential for porous media. *International Journal of Engineering Science*. 34(14). p.1611-1621.

Bennethum, L.S., Murad, M.A., Cushman, J.H. (1997) Modified Darcy's Law, Terzaghi's Effective Stress Principle and Fick's Law for swelling clay soils. *Computers and Geotechnics*. 20. p.245-266.

Besq, A., Malfoy, C., Pantet, A., Monnet, P., Righi, D. (2003) Physiochemical characterisation and flow properties of some bentonite muds. *Applied Clay Science*. 23 (5). p.275-286.

Bleam, W.F. (1993) Atomic theories of phyllosilicates: Quantum chemistry, statistical mechanics, electrostatic theory, and crystal chemistry. *Revies of Geophysics*. 31 (1). p.51-73.

Boek, E.S., Coveney, P.V., Skipper, N.T. (1995) Monte Carlo molecular modeling studies of hydrated Li-, Na-, and K-smectites: Understanding the role of potassium as a clay swelling inhibitor. *Journal of the American Chemical Society*. 117. p.12608-12617.

Celia, M.A., Bouloutas, E.T., Zarba, R.L. (1990) A general mass-conservative numerical solution for the unsaturated flow equation. *Water Resources Research*. 26 (7). p.1483-1496.

Chamley, H. (1989) *Clay Sedimentology*. New York: Springer-Verlag Berlin Heidelberg.

Chang, F.R.C., Skipper, N.T., Sposito, G. (1997) Monte Carlo and molecular dynamics simulations of interfacial structure in lithium-montmorillonite hydrates. *Langmuir*. 13. p.2074-2082.

Chang, F.R.C., Skipper, N.T., Sposito, G. (1998) Monte Carlo and molecular dynamics simulations of electrical double-layer structure in potassium-montmorillonite hydrates. *Langmuir*. 14. p.1201-1207.

Chávez-Páez, M., Van Workum, K., de Pablo, L. (2001) Monte Carlo simulations of Wyoming sodium montmorillonite hydrates. *The Journal of Chemical Physics*. 114 (3). 1405-1413.

Cui, X., Bustin, R.M. (2005) Volumetric strain associated with methane desorption and its impact on coalbed gas production from deep coal seams. *American Association of Petroleum Geologists*. 89 (9). p.1181-1202.

Erdogan, A.R. (2016) *Interpretation of clay swelling via non-contact linear displacement meter (NC-LDM)*. A thesis submitted for the degree of Master of Science by Research. Durham University.

Foo, K.Y., Hameed, B.H. (2010) Insights into the modeling of adsorption isotherm systems. *Chemical Engineering Journal*. 156. p.2-10.

Franklin, J.A., Dusseault, M.B. (1989) *Rock engineering*. California: McGraw-Hill.

Goudarzi, S., Mathias, S.A., Gluyas, J.G. (2016) Simulation of three-component two-phase flow in porous media using method of lines. *Transport in Porous Media*. 112. p.1-19.

Guéguen, Y. & Boutéca, M. (2004) *Mechanics of fluid-saturated rocks*. Massachusetts: Elsevier Academic Press.

Hassanizadeh, S.M., Gray, W.G. (1979) General conservation equations for multi-phase systems: 1. Averaging procedure. *Advances in Water Resources*. 2. p.131-144.

Hassanizadeh, S.M., Gray, W.G. (1990) Mechanics and thermodynamics of multiphase flow in porous media including interphase boundaries. *Advances in Water Resources*. 13(4). p.169-186.

Hensen, E.J.M., Smit, B. (2002) Why clays swell. *Journal of Physical Chemistry B.* 106. p.12664-12667.

IEA (2015) *Key world energy statistics.* IEA. Paris.

IEA (2016) *Key world energy trends: Excerpt from world energy balances.* IEA. Paris.

Jaeger, J.C., Cook, N.G.W., Zimmerman, R.W. (2007) *Fundamentals of rock mechanics.* Fourth edition. Massachusetts: Blackwell Publishing.

Karaborni, S., Smit, B., Heidug, W., Urai, J., van Oort, E. (1996) The swelling of clays: Molecular simulations of the hydration of montmorillonite. *Science.* 271. p.1102-1104.

Kukol, A. (2008) *Molecular modeling of proteins.* New Jersey: Humana Press.

Lal, M. (1999) Shale stability: Drilling fluid interaction and shale strength. In *Society of Petroleum Engineers Latin American and Caribbean Petroleum Engineering Conference.* Caracas, Venezuela, 21st to 23rd April 1999.

Lemon, G., King, J.R., Byrne, H.M., Jensen, O.E., Shakesheff, K.M. (2006) Mathematical modelling of engineered tissue growth using a multiphase porous flow mixture theory. *Journal of Mathematical Biology.* 52(5). p.571-594.

Levine, J.R. (1996) Model study of the influence of matrix shrinkage on absolute permeability of coal bed reservoirs. *Coalbed Methane and Coal Geology.* 109. p.197-212.

Limousin, G., Gaudet, J.P., Charlet, L., Szenknect, S., Barthès, V., Krimissa, M. (2007) Sorption isotherms: A review on physical bases, modeling and measurement. *Applied Geochemistry.* 22. p.249-275.

Lu, N. & Likos, W.J. (2004) *Unsaturated soil mechanics.* New Jersey: John Wiley & Sons, Inc.

Mathias, S.A., Butler, A.P., Zhan, H. (2008). Approximate solutions for Forchheimer flow to a well. *Journal of Hydraulic Engineering.* 134 (9). p.1318-1325.

Murad, M.A., Bennethum, L.S., Cushman, J.H. (1995) A multi-scale theory of swelling porous media: 1. Application to one-dimensional consolidation. *Transport in Porous Media.* 19. p.93-122.

Norrish, K. (1954) The swelling of montmorillonite. *Discussions of the Faraday Society.* 18. p.120-134.

Palmer, I., Mansoori, J. (1998) How permeability depends on stress and pore pressure in coalbeds: A new model. *SPE Reservoir Evaluation & Engineering.* p.539-544.

Pillalamarry, M., Harpalani, S., Liu, S. (2011) Gas diffusion behaviour of coal and its impact on production from coalbed methane reservoirs. *International Journal of Coal Geology.* 86. p.342-348.

Schaap, M.G., Leij, F.J., van Genuchten, M.T. (2001) ROSETTA: A computer program for estimating soil hydraulic parameters with hierarchical pedotransfer functions. *Journal of Hydrology.* 251. p.163.176.

Schwartz, F.W. & Zhang, H. (2003) *Fundamentals of groundwater.* New York: John Wiley & Sons, Inc.

Shampine, L.F. & Reichelt, M.W. (1997) The MATLAB ODE suite. *SIAM Journal on Scientific Computing.* 18 (1). p.1-22.

Shi, J.Q., Durucan, S. (2004) Drawdown induced changes in permeability of coalbeds: A new interpretation of the reservoir response to primary recovery. *Transport in Porous Media*. 56. p.1-16.

Skipper, N.T., Lock, P.A., Titiloye, J.O., Swenson, J., Mirza, Z.A., Howells, W.S., Fernandez-Alonso, F. (2006) The structure and dynamics of 2-dimensional fluids in swelling clays. *Chemical Geology*. 230. p.182-196.

Skipper, N.T., Sposito, G., Chang, F.R.C. (1995) Monte Carlo simulation of interlayer molecular structure in swelling clay minerals. 2. Monolayer hydrates. *Clays and Clay Minerals*. 43 (3). p.294-303.

Smith, D.E., Wang, Y., Chaturvedi, A., Whitley, H.D. (2006) Molecular simulations of the pressure, temperature and chemical potential dependencies of clay swelling. *Journal of Physical Chemistry B*. 110. p.20046-20054.

Suter, J.L., Anderson, R.L., Greenwell, H.C., Coveney, P.V. (2009) Recent advances in large-scale atomistic and coarse-grained molecular dynamics solution of clay minerals. *Journal of Materials Chemistry*. 19. p.2482-2493.

Tambach, T.J., Hensen, E.J.M., Smit, B. (2004) Molecular simulations of swelling clay minerals. *Journal of Physical Chemistry B*. 108. p.7586-7596.

Tucker, M.E. (2001) *Sedimentary Petrology: An introduction to the origin of sedimentary rocks*. Third edition. Oxford: Blackwell Science Ltd.

van Genuchten, M.T. (1980) A closed-form equation for predicting the hydraulic conductivity of unsaturated soils. *Soil Science Society of America Journal*. 44. p.892-898.

Varado, N., Braud, I., Ross, P.J., Haverkamp, R. (2006) Assessment of an efficient numerical solution of the 1D Richards' equation on bare soil. *Journal of Hydrology.* 323. p.244-257.

Watson, F.E., Mathias, S.A., van Hunen, J., Daniels, S.E., Jones, R.R. (2012) Dissolution of CO_2 from leaking fractures in saline formations. *Transport in Porous Media.* 94. p.729-745.

Weinstein, T.F., Bennethum, L.S., Cushman, J.H. (2008) Two-scale, three-phase theory for swelling drug delivery systems. Part 1: Constitutive theory. *Journal of Pharmaceutical Science.* 97. p.1878-1903.

Wilson, M.J., Wilson, L. (2014) Clay mineralogy and shale instability: An alternative conceptual analysis. *Clay Minerals.* 49. p.127-145.

Zadeh, K.S. (2011) A mass-conservative switching algorithm for modeling fluid flow in variably saturated porous media. *Journal of Computational Physics.* 230. p.664-679.

Zhang, L.M., Sun, B.W. (1999) Inhibition of water-soluble cationic cellulosic polymers to clay hydration. *Journal of Applied Polymer Science.* 74. p.3088-3093.